MMP13 and TIMP1 are functional markers for two different potential modes of action by mesenchymal stem/stromal cells when treating osteoarthritis

Anna Salerno[1], Kyla Brady[1], Margot Rikkers[1,2], Chao li[1], Eva Caamaño-Gutierrez[3,4], Francesco Falciani[3,4], Ashley W. Blom[5,6], Michael R. Whitehouse[5,6] and Anthony P. Hollander[1]

Running title: Functional markers of mesenchymal stem cells

[1]Institute of Lifecourse and Medical Sciences, University of Liverpool, UK

[2]Department of Orthopaedics, University Medical Center Utrecht, The Netherlands

[3]Institute of Systems, Molecular and Integrative Biology, University of Liverpool, UK

[4]Computational Biology Facility, University of Liverpool, UK

[5]Musculoskeletal Research Unit, University of Bristol, UK

[6]National Institute for Health Research Bristol Biomedical Research Centre, University Hospitals Bristol NHS Foundation Trust and University of Bristol, UK

AUTHOR CONTRIBUTONS:

AS: Collection and/or assembly of data, data analysis and interpretation, manuscript writing; KB: Collection and/or assembly of data, data analysis and interpretation, manuscript writing; MR: Collection and/or assembly of data, manuscript writing; CL: Collection and/or assembly of data, manuscript writing; ECG: Data analysis and interpretation, manuscript writing; FF: Data analysis and interpretation, manuscript writing; AWB: Provision of study material or patients, manuscript writing; MRW: Provision of study material or patients, manuscript writing; APH: Conception and design, financial support, data analysis and interpretation, manuscript writing

Correspondence:
Anthony P. Hollander PhD, Institute of Lifecourse and Medical Sciences, William Henry Duncan Building, University of Liverpool, 6 West Derby Street, Liverpool, L7 8TX
Email: A.Hollander@Liverpool.ac.uk

Funding information
This work was supported by a grant from Innovate UK [grant number: 102164]. M.R. was funded by an Erasmus+ Traineeship mobility grant [student number: 3930572].

KEYWORDS
Mesenchymal stem cells, chondrogenesis, trophic repair, MMP13, TIMP1

ABSTRACT

Mesenchymal stem cells (MSCs) have been investigated as a potential injectable therapy for the treatment of knee osteoarthritis, with some evidence of success in preliminary human trials. However, optimisation and scale-up of this therapeutic approach depends on the identification of functional markers that are linked to their mechanism of action. One possible mechanism is through their chondrogenic differentiation and direct role in neo-cartilage synthesis. Alternatively, they could remain undifferentiated and act through the release of trophic factors that stimulate endogenous repair processes within the joint. Here, we show that extensive *in vitro* ageing of bone-marrow-derived human MSCs leads to loss of chondrogenesis but no reduction in trophic repair, thereby separating out the two modes of action. By integrating transcriptomic and proteomic data using Ingenuity Pathway Analysis, we found that reduced chondrogenesis with passage is linked to downregulation of the FOXM1 signalling pathway whilst maintenance of trophic repair is linked to CXCL12. In an attempt at developing functional markers of MSC potency, we identified loss of mRNA expression for MMP13 as correlating with loss of chondrogenic potential of MSCs and continued secretion of high levels of TIMP1 protein as correlating with the maintenance of trophic repair capacity. Since an allogeneic injectable OA therapy would require extensive cell expansion *in vitro*, we conclude that early passage MMP13^{+}, TIMP1-secreting^{high} MSCs should be used for autologous OA therapies designed to act through engraftment and chondrogenesis, whilst later passage MMP13^{-}, TIMP1-secreting^{high} MSCs could be exploited for allogeneic OA therapies designed to act through trophic repair.

1. INTRODUCTION

The concept of multipotent mesenchymal stem cells (MSCs) was established by Caplan in the early 1990s [1] following the seminal work of Friedenstein in the 1960s and 1970s, demonstrating the presence of osteogenic precursor cells in bone marrow [2-4]. Building on this early work, there have been many studies demonstrating the capacity of MSCs to differentiate *in vitro* with clear evidence for multipotent skeletal lineage differentiation [5], including chondrogenesis [6-13], osteogenesis [14-17], and adipogenesis [9, 18, 19] as well as more limited evidence for pluripotent differentiation including endodermal and ectodermal pathways [1, 20]. In one of these studies, we generated clonal populations of bone marrow MSCs and showed that individual cells retained the capacity for chondrogenesis, with varying degrees of potency [9].

More recently, evidence has grown that MSCs may support tissue repair through mechanisms that do not directly relate to their multipotential differentiation capacity [21]**.** Caplan has described MSCs as having "trophic" capacity by which, following implantation, they induce neighbouring cells to secrete active molecules, for example in the treatment of stroke, myocardial infarction or in meniscal cartilage repair [22]. Trophic repair is most likely mediated through the production by MSCs of large amounts of growth factors and other mediators [20, 22-25]. We have previously developed a therapeutic strategy for meniscal cartilage repair based on the trophic properties of MSCs [26] that has shown some evidence of efficacy in pre-clinical and clinical trials [27]. A second mechanism contributing to trophic repair is the ability of MSCs to suppress immune responses by a range of mechanisms including downregulation of T cell proliferation [9, 24, 28-31]. This important

property of MSCs has been used clinically to support the engraftment of donated haematopoetic cells and to prevent graft versus host disease [24, 32].

There have been several studies describing the loss of differentiation capacity with increasing passage of MSCs *in vitro* [33-36], with other studies suggesting that *in vivo* ageing also leads to a loss of differentiation capacity after *ex vivo* isolation of the aged cells [37-39]. These observations combined with parallel observations of shortening in telomere length with *in vitro* ageing of MSCs [40] have been interpreted as indicating a rapid senescence process that compromises cell function and limits their clinical utility. Conversely, no comparative ageing-related data have been reported for trophic repair or immunoregulation.

The aim of this study was to identify markers of MSC chondrogenic potency (measured by cartilage tissue engineering) and trophic potency (measured by meniscal cartilage integration as well as by suppression of T-cell proliferation), using extensive *in vitro* ageing of the cells as a method of regulating their specific functional activity.

2. MATERIALS AND METHODS

2.1. Isolation and expansion of human marrow derived MSCs for *in vitro* studies

The model used as the basis for all the experiments reported here was long-term culture of human bone-marrow derived MSCs. Bone marrow plugs were collected from the femoral heads of patients undergoing total hip replacement. All patients gave their informed consent and the study was carried out according to local ethical guidelines (North Bristol NHS Trust Research Ethics Committee). Patient details can be seen in Table S1. Cells were suspended in stem cell expansion medium consisting of low glucose Dulbecco's Modified Eagles Medium (Sigma-Aldrich) supplemented with 10% (v/v) Foetal Bovine Serum (FBS, Sigma-Aldrich), 1% (v/v) Glutamax (Gibco) and 1% (v/v) Penicillin/Streptomycin (Sigma-Aldrich). The serum batch was selected to promote the growth and differentiation of MSCs [41]. The medium was also supplemented with 10 ng/ml FGF-2 (Peprotech). This growth factor has been previously shown to enhance the MSC proliferation rate *in vitro* [12, 42], to retain MSCs as undifferentiated cells during proliferation [6, 43] and to enhance chondrogenic differentiation when the FGF-2 expanded MSCs are subsequently exposed to differentiation conditions [12, 42]. The cell suspension was separated from any bone in the sample by repeated washing with media. The cells were centrifuged at 500 *g* for 5 minutes and the supernatant/fat removed. The resulting cell pellet was resuspended in medium, and then plated at a seeding density of between 1.5-2.0x10^5 nucleated cells per cm^2. These flasks were incubated at 37°C in a humidified atmosphere of 5% CO_2 and 95% air. Four days were allowed before the first medium change and then the medium was changed every other day until adherent cells reached 90% confluence and were ready for passaging.

2.2. Cell passaging and calculation of population doublings and doubling time

At the end of each passage the MSCs were harvested using 0.25% trypsin-EDTA (Sigma-Aldrich), pooled, counted and then divided into different centrifuge tubes for reseeding and further growth, for immediate use in measurement of % integration of meniscal cartilage, for storage in liquid nitrogen for subsequent use in differentiation protocols as well as for genomic and proteomic analysis. The cells for each patient were passaged continuously without freezing, until growth arrest, defined as no detectable increase in cell number between passages (See Table S1). At each passage, the total number of harvested MSCs was determined. The first cell harvest after seeding of fresh bone marrow was taken as passage 0. The number of cells reseeded at the start of Passage 1 was used as the baseline for calculation of the first population doubling value at the end of passage 1. Downstream analyses of the MSCs were undertaken from passage 1 onwards.

The number of Population doublings (PDs) was calculated using the following formula:

$$PDs = [\log(\text{Number of Harvested MSCs}) - \log(\text{Number of seeded MSCs})]/\log(2)]$$

The PD for each passage was calculated and added to the PD of the previous passages to generate data for Cumulative PD at each Passage.

Population doubling time (PDT) was calculated for each passage using the formula:

$$PDT = t \times \log(2)/\log(\text{cells harvested}/\text{cells seeded})$$

(t = the time between cell seeding and cell harvesting)

2.3. Detection of cell-surface phenotypic markers

MSCs (100,000 cells from each patient at each of passages 1, 5, 10 and 15) were suspended in a 1:500 dilution of Zombie (Biolegend), a live/dead cell dye, and incubated for 20mins in the dark. Nonspecific antigens were then blocked by incubating the cells at room temperature for 1 hour in 1% (wt/vol) Bovine Serum Albumen (BSA; Sigma-Aldrich), 5% (vol/vol) FBS. The cells were washed by centrifugation in three volumes of Sulbecco's Phosphate Buffered Saline (PBS; Sigma-Aldrich), and the cell pellet was suspended in 100µl of a primary antibody solution containing 20–100µg/ml of antibody in blocking solution. All the primary antibodies were fluorescent-labelled mouse anti-human IgGs: anti-CD105-fluorescein isothiocyanate (FITC), anti-CD90-phycoerythrin (PE), anti-CD45-PE were from R&D Systems); anti-CD34-FITC was from eBioscience, Life Technologies; IgG1-FITC and IgG1-PE isotype controls were from R&D Systems. After incubation for 40 minutes at 4°C, the cells were washed and suspended in 1 ml of PBS for analysis on a Canto flow cytometer (BD FACSCanto II), after the exclusion of non-viable cells. Data were analysed using FlowJo (Treestar). Positive expression was defined as the level of fluorescence greater than 95% of corresponding isotype-matched control antibodies.

2.4. Chondrogenesis

Cartilage tissue engineering

The chondrogenic capacity of MSCs from each passage were assessed by performing three-dimensional cartilage tissue engineering, as previously described [41]. Briefly, 300,000 cells were loaded drop-wise onto 5 mm diameter x 2 mm thick polyglycolic acid (PGA) scaffold discs (Biomedical Structures) which had been pre-coated with 100 µg/ml fibronectin (Sigma-

Aldrich). Constructs were then cultured in chondrogenic differentiation medium consisting of DMEM containing 4500 mg/L (high) glucose (Sigma-Aldrich), supplemented with 10 ng/ml transforming growth factor-β3 (TGF-β3; R&D Systems), 100 nM dexamethasone, 80 µM ascorbic acid 2-phosphate, 1 mM sodium pyruvate, 1% (v/v) Penicillin/Streptomycin (all from Sigma-Aldrich), 1% insulin-transferrin-selenium-G (ITS) and 2 mM Glutamax (both from Gibco). After 7 days, the medium was further supplemented with 10 µg/ml human insulin (Sigma-Aldrich) until the end of culture. The constructs were incubated at 37°C for a total of 35 days on a rotating platform and medium was changed every three days.

Biochemical analysis

Cartilage constructs were freeze-dried and weighed at the end of the 35-day tissue engineering period. The extracellular matrix was fully solubilised by overnight digestion with 2 mg/ml bovine pancreatic trypsin (Sigma-Aldrich) which was then boiled for 15 min to inhibit the action of the enzyme [44]. In order to obtain the dry weight of extracellular matrix in the construct, remaining undigested scaffold material was freeze-dried, weighed and subtracted from the original dry weight. The amounts of proteoglycan in the digests was measured as sulphated glycosaminoglycan (GAG) using a dimethylmethylene blue (Sigma-Aldrich) colorimetric assay [45].

2.5. Osteogenesis and adipogenesis

Whole MSC populations or MSC clones were grown in monolayer until 50-70% confluent prior to osteogenic differentiation or 100% confluent prior to adipogenic differentiation. In both cases, control cells were then cultured in Minimum Essential Medium (α-MEM; Sigma-Aldrich) basal medium containing 10% FBS, 1% (v/v) Penicillin/Streptomycin and 2 mM

Glutamax. Cells stimulated to undergo differentiation were cultured in basal medium containing either Osteogenic Supplement or Adipogenic Supplement (both from R&D Systems) for 21 days. Following osteogenic differentiation cells were fixed in 70% ethanol and stained with 40 mM alizarin red S (Sigma-Aldrich), pH4.1, for 5 min. Following adipogenic differentiation cells were fixed in 4% paraformaldehyde and stained with 0.3% oil red O (Sigma-Aldrich) for 30 min. The extent of differentiation was scored under blind conditions and classified as - (no staining), +, ++ or +++ according to increasing area and number of mineralised deposits following osteogenic differentiation (See **Figure S1**) and increasing number of lipid droplets following adipogenic differentiation (see **Figure S3**).

2.6. Meniscal repair

Preparation of sheep meniscal cartilage

Sheep legs were purchased from Edge & Son Butchers, Wirral, Merseyside and the meniscal cartilage removed under sterile conditions. Meniscal cartilage cylinders (5.0 mm in diameter and 3.0 mm thick) were harvested from the avascular (white zone) of the ovine menisci using a dermal biopsy punch. They were rinsed and incubated with PBS containing 10% (v/v) Penicillin/Streptomycin and 1% (v/v), 250µg/ml Amphotericin B (Sigma-Aldrich) for 20 minutes. Viability of the fibrocartilage discs was maintained by culture in basic medium consisting of low-glucose DMEM with 10mM Hepes buffer (Sigma-Aldrich), 1% (v/v) Penicillin/Streptomycin, non-essential amino acids (NEAA; Sigma-Aldrich), 1% (v/v) Glutamax and 10% amphotericin B at 37°C in a 5% CO_2 environment. The explants were used in the integration experiments within 3 days of culture.

Cell seeding

Collagen scaffolds (Ultrafoam Collagen Sponge; Bard) were cut into 6mm diameter discs and seeded with human MSCs at a concentration of 1 x 10^6 cells/cm^2. The suspension was loaded drop wise onto the scaffold placed in ultra-low attachment wells of a 24-well plate (Corning). After 4 hours, 1.5 ml of expansion medium containing 10 ng/ml FGF-2 was added and changed daily. Seeded scaffolds were incubated for 48 hours at 37°C in an orbital shaker at 50 rpm.

Assembling and culture of constructs

Sandwich constructs of two ovine meniscal cartilage discs interposed with a seeded scaffold were assembled as previously described [27] using skin clips and cultured *in vitro* in ultra-low attachment 6-well plates in expansion medium with 10 ng/mL FGF-2 for 7 days followed by culture in an integration medium consisting of high glucose DMEM containing 10% (v/v) FBS, 1% (v/v), Glutamax, 1% (v/v) Penicillin/Streptomycin, insulin and 80 µM ascorbic acid 2-phosphate for 33 days. The medium was replenished twice every week. The constructs were incubated at 37°C on a rotating platform throughout the culture period. At the end of culture, the constructs were prepared for histological analysis by fixation in 10% (v/v) neutral buffered formalin (Sigma-Aldrich).

Histomorphometric analysis

Histomorphometry was carried out using a method that we developed and characterized in previous studies [27, 46, 47]. Fixed constructs were dehydrated and paraffin embedded. Samples were cut into 4µm sections and stained with hematoxylin and eosin (H&E) for the study of morphological details. All histological sections were scanned using a Leica Aperio

slide scanner and histomorphometric analysis was performed under blind conditions, using ImageScope software (Leica). Two perpendicular sections, one at the edge and another one at the center of each construct were used. For each section, the entire length of the implant/meniscus interface was measured, as well as the length of any areas of integration at the interface. The repair index was then determined as:

$$\% \text{ Integration} = \text{Length of integrated interface} / \text{Total interface length} \times 100$$

2.7. Immunosuppression

Human peripheral blood mononuclear cells (PBMCs) were isolated from donor blood samples from healthy volunteers. All the volunteers gave their informed consent and the study was carried out according to local ethical guidelines (University of Liverpool Research Ethics sub-committee for Physical Interventions). PBMCs were isolated by centrifugation of the blood on 1.077 g/mL Ficoll-Paque PLUS (GE Healthcare Life Sciences) and cultured in RPMI-1640 containing L-glutamine (Sigma-Aldrich) and supplemented with 10% Human AB Serum (Sigma-Aldrich) and 1% (v/v) Penicillin/Streptomycin. PBMCs were stained with CellTrace™ Violet (ThermoFisher) to monitor T-cell proliferation. Labelled PBMCs were then stimulated with 3.75µg/ml anti-human CD3 (HIT3a) and 2µg/ml anti-human CD28 (CD28.2) (both from Fisher Scientific Affymetrix eBioscience) and co-cultured with MSCs from 4 individual donors at passages 1, 5, 10 and 15 for 72 hours. The T-cell proliferation profile for each population was analysed by flow cytometry following exclusion of non-viable cells stained with 7-amino-actinomycin D (7-AAD; BD Biosciences).

2.8. Quantitative PCR

Real-time quantitative PCR (RT-qPCR) for MMP13 mRNA and for the housekeeping gene Tata Binding Protein (RBP) were performed using the CellsDirect™ One-Step qRT-PCR Kit (ThermoFisher), with which reverse transcription and PCR amplification were performed in the same reaction tube. Primers specific for MMP13 (Hs00942584_m1) and TBP (Hs00427621_m1) were purchased from ThermoFisher TaqMan®. The reaction was started by synthesisizng cDNA at 50°C for 15min, followed by 2min at 95°C to denature RNA-cDNA hybrids and deactivate reverse transcriptase. The thermal cycling program consisted of 50°C for 15 minutes, 95°C for 2 minutes, and 40 two-step cycles of 95°C for 10s and 60°C for 30s. MMP13 expression relative to TBP was determined at each of 4 time points for each MSC sample and the results normalised to the time (passage 2), which was taken as a Fold-expression of 1.0.

2.9. TIMP-1 ELISA

TIMP-1 protein was measured in the secretome of MSCs using the Quantikine® ELISA Kit for human TIMP-1 (R&D Systems). MSCs were seeded into 6-well plates at 2.25 million cells/well (3 replicates) and cultured in 2ml of DMEM for 24 h. The medium was then replaced with 1 ml of phenol-free culture medium for a further 24h, after which the secretome was collected and assayed at appropriate dilution using the ELISA kit.

2.10. Acquisition of genomic and proteomic data

Transcriptomics

Transcriptomics was performed by the Centre for Genomic Research on mRNA extracted from the mRNA of all four patients at P1, P5, P10 and P15. When MSCs were harvested at

the end of each passage, $1x10^6$ cells were isolated and resuspended in RNAprotect Cell Reagent (Qiagen). The cells were stored at -80°C until the complete set of samples from all donors and time points had been collected. RNA was then extracted from selected time points using the RNeasy Plus Mini Kit (Qiagen), according to the manufacturer's instructions. The concentration of RNA in the extract was determined using a NanoDrop 2000 spectrophotometer (Thermo). Extracted RNA was stored at -80°C prior to analysis.

Ribosomal RNA depletion was performed using the Ribo-Zero™ H/M/R Kit (New England Biolabs) and RNASeq libraries were then prepared using the NEB Next Ultra Directional RNA Library Prep Kit (New England Biolabs). Paired-end sequencing of the RNASeq libraries was performed by the Illumina HiSeq4000 platform using V4 chemistry.

Proteomics

Proteomics was performed on secretome prepared from the MSCs of all four patients at P1, P5, P10 and P15. When MSCs were harvested at the end of each passage, $1x10^6$ cells were isolated and resuspended in 4 mL of serum-free, phenol red-free DMEM supplemented with 4500 mg/L (high) glucose (Sigma-Aldrich), 1% (v/v) Glutamax, 1% (v/v) and Penicillin/Streptomycin for 24 hours at 37°C. The conditioned medium recovered at the end of the incubation was harvested from each flask and stored at -80°C prior to analysis.

Proteomic analyses of the secretome samples was undertaken in the "Centre for Proteome Research" facility at the University of Liverpool. Protein solutions were concentrated by adding consecutive 1 mL aliquots of each sample to 10µL of Strataclean beads (Agilent).

After each aliquot had been added, the sample was vortexed for 1 minute, centrifuged at 2,000 x g for 2 minutes and the protein-depleted supernatant removed. After the final aliquot had been added, the beads were washed two times with 1 mL of 25mM ammonium bicarbonate (ambic) prior to digestion. For on-bead digestion, the beads were re-suspended in 80µL of 25 mM ambic and 5µL of 1%(w/v) Rapigest (Waters) was added. The samples were heated at 80°C for 10 minutes and then reduced by the addition of 5 µL of 9.2mg/mL dithiothreitol (DTT; Roche) in 25mM ambic and heating at 60°C for 10mins. Following cooling, 5 µL of 33mg/ml iodoacetamide (Sigma-Aldrich) in 25mM ambic was added and the samples incubated at RT for 30min in the dark. Porcine trypsin (sequencing grade, Promega) (1µg) was added and the sample was incubated at 37°C overnight on a rotary mixer. The digests were acidified by the addition of 1 µL of trifluoracetic acid (TFA) and incubated at 37°C for 45 minutes. Samples were then centrifuged at 17,200 x g for 30mins and supernatants transferred to 0.5 mL low-binding tubes. They were centrifuged for a further 30mins and 10µL transferred to total recovery vials for LC-MS analysis.

Data-dependent LC-MSMS analyses were conducted on a QExactive HF quadrupole-Orbitrap mass spectrometer coupled to a Dionex Ultimate 3000 RSLC nano-liquid chromatograph (Hemel Hempstead, UK). Sample digest (1-2µL) was loaded onto a trapping column (Acclaim PepMap 100 C18, 75µm x 2cm, 3µm packing material, 100Å) using a loading buffer of 0.1%(v/v) TFA, 2%(v/v) acetonitrile in water for 7 minutes at a flow rate of 12µL min^{-1}. The trapping column was then set in-line with an analytical column (EASY-Spray PepMap RSLC C18, 75µm x 50cm, 2µm packing material, 100Å) and the peptides eluted using a linear gradient of 96.2% A (0.1 %[v/v] formic acid): 3.8% B (0.1% [v/v] formic acid in water: acetonitrile [80:20] [v/v]) to 50% A:50% B over 90min at a flow rate of 300nL min^{-1}, followed

by washing at 1% A : 99% B for 5 minutes and re-equilibration of the column to starting conditions. The column was maintained at 40°C, and the effluent introduced directly into the integrated nano-electrospray ionisation source operating in positive ion mode. The mass spectrometer was operated in DDA mode with survey scans between *m/z* 350-2000 acquired at a mass resolution of 60,000 (FWHM) at *m/z* 200. The maximum injection time was 100ms, and the automatic gain control was set to 3e6. The 16 most intense precursor ions with charges states of between 2+ and 5+ were selected for MS/MS with an isolation window of 2*m/z* units. The maximum injection time was 45ms, and the automatic gain control was set to 1e5. Fragmentation of the peptides was by higher-energy collisional dissociation using a normalised collision energy of 30%. Dynamic exclusion of *m/z* values to prevent repeated fragmentation of the same peptide was used with an exclusion time of 20s. Raw data files from the mass spectrometry were imported into Progenesis QI for Proteomics v.2.0 software (Waters Ltd, Newcastle upon Tyne, UK) for alignment and peak detection. An aggregate file was generated which contained all the peaks from all runs in an experiment so that there were no missing values. The data was filtered and charges +1 and ≥+8 were removed. The msms fragmentation data was searched against the UniProt human reviewed DB using Mascot v. 2.4.1 software (Matrix Science, London, UK). The precursor ion mass tolerance was set to 10ppm and the product ion tolerance to 0.01Da. Oxidation of methionine was selected as a dynamic modification and carbamidomethyl cysteine as a fixed modification. One missed cleavage was permitted. The Mascot search returned 2,594 proteins at 2.17% FDR (psms above homology). A 1%FDR was set and 2,366 proteins were exported as an .xml file (FDR type: distinct psms) and imported into Progenesis and peptides assigned to proteins. Protein quantification was based on averaging the individual

abundances for each protein per donor at each passage and comparing proteins that were differentially expressed between the 4 passages.

2.11. QUANTIFICATION AND STATISTICAL ANALYSIS

Bioinformatics

Data processing, integration and analyses were undertaken by the Computational Biology Facility at the University of Liverpool. RNAseq data was acquired as described above. The raw Fastq files were trimmed for the presence of Illumina adapter sequences using Cutadapt version 1.2.1, option –O 3. Reads were further trimmed using Sickle version 1.200 with a minimum window quality score of 20. Reads shorter than 10 base pairs after trimming were removed. Sequence quality metrics were assessed using FastQC version 0.11.4. No samples were removed. Sequence data were aligned to the human genome version GRCh38 from NCBI using Bowtie2 version 1.1.2 with recommended parameters [48]. Gene level count data were generated from the Bowtie2 alignments using htseq-count version 0.9.0. The R library DESeq2 was used to produced rlog transformed count data. These were filtered to remove genes with less than 1 average count. Statistical analyses were performed in R version 3.4.4 and graphical representations were done using the R package ggplot2.

Normalised proteomics and transcriptomics data were integrated and preliminary exploratory analyses revealed a relevant heterogeneity between patients. In order to discriminate between changes related to patient heterogeneity and changes related to passage, differentially expressed variables over passage were calculated with a 2-way ANOVA to account for patient variability as confounder. This followed multiple testing

correction using the Benjamin-Hochberg method. Significant variables (338 of which 38 were proteins and 300 were genes) uniquely over passage were selected for further analysis in the Ingenuity Pathway Database (IPA, Qiagen, Analysis 2015).

Base 2 log fold changes of the 338 significant variables were calculated with respect to passage 1 and used for a IPA (Qiagen), where analysis was performed according to the manual to predict possible upstream regulators involved in the changes observed, possible pathways affected and a number of functions and terms significantly enriched (database access on the 9th of December 2018). IPA was also used to download knowledge terms involved in selected key processes, i.e. (A) Cell migration in mesenchymal stem cells (B) cell movement in mesenchymal stem cells and (C) wound healing. All these variables were mapped to our experimental data. Then we assessed the number of variables changing over passage within these terms and contextualise the biological findings.

Principal Component Analysis was performed in mean centred and scaled data via singular value decomposition using the function prcomp within the statistical software R.

Statistics

Differentiation variables (TE, GAG, and osteogenesis and adipogenesis scores) were compared over passage by calculating the non-parametric Spearman correlation embedded in the function cor.test within the stats package in R. Osteogenesis and adipogenesis capabilities were measured with semi quantitative data based on image analysis. These were translated into integers 0 to 1 to undertake the calculation.

Data availability

The accession number for the RNA-seq data reported in this paper and deposited at the NCBI Gene Expression Omnibus (GEO) database is: GSE137186

The proteome data reported in this paper has been deposited at the Figshare database and can be downloaded from: **https://doi.org/10.6084/m9.figshare.12317123.v1**

3. RESULTS

3.1. Patient characteristics and MSC growth potential

Bone marrow was collected from patients undergoing knee or hip arthroplasty. All patients gave informed consent and the study was performed in full accordance with local ethics guidelines (Southmead Research Ethics Committee Ref 078/01). **Table S1** shows the patient characteristics. All four were male with a mean age of 49 years (range, 38-70 years) at the time of operation. MSCs where isolated from each bone marrow by plastic adhesion and grown under standard culture conditions until they failed to proliferate any further. MSCs from PN241 and PN242 continued to proliferate for a larger number of passages than MSCs from PN251 and PN264, with PN242 cells showing no sign of growth arrest even at passage 30 (**Figure 1A and Table S1**). **Figure 1B** shows the MSC population doubling time (PDT) at each passage for each patient up to passage 17. The PDT of MSCs from all four patients was similar at early passages and became longer at later passages, with MSCs from one patient (PN264) showing particularly slow growth at higher passage numbers. . Early passage MSCs had a typical small size and stellate appearance, but became larger and less spindly as the cells became more senescent (**Figure 1C, PN251**). However, PN242 cells had a small size and spindly, stellate appearance even at very high passage number, when they were continuing to proliferate well (**Figure 1C, PN242**). These results are consistent with previous studies showing that cell enlargement and loss of stellate shape are associated with increased senescence [34].

Cell surface marker expression was determined by FACS using MSCs from all four patients at each of passages P1, P5, P10 and P15. The expression of MSC markers CD105 and CD90 was maintained at >90% at late passage in MSCs from all four patients. Haematopoetic stem cell marker CD45 remained at <10% at all passages however there was a small increase in the expression of haematopoetic stem cell marker CD34 with increasing passage number in two of the patients (**Figure 1D**).

3.2. The tri-lineage differentiation potential of MSCs falls with increasing passage

MSCs from selected passages of each patient were tested for their chondrogenic potential in a three-dimensional cartilage tissue engineering assay, with the amount of engineered cartilage measured as the dry weight of tissue and quality of the cartilage measured as the glycosaminoglycans content expressed as a % of dry weight. There was clear evidence of a loss of chondrogenic potential with *in vitro* ageing of the cells. The typical macroscopic appearance of tissue engineered cartilage over a range of passages for MSCs from each of the patients can be seen in **Figure 2**, clearly demonstrating a reduction in the average size of cartilage constructs when produced using late passage MSCs. This macroscopic observation was supported by quantitative analysis. There was a significant negative correlation between the mean dry weight of cartilage formed and the cumulative population doublings of MSCs recorded at the time of tissue engineering for three out of the four patients and a significant negative correlation between the mean cartilage glycosaminoglycans content and the cumulative population doublings of MSCs recorded at the time of tissue engineering for all four patients (**Figures 3A-D**). Furthermore, both the dry weight and the glycosaminoglycans content of all the individual tissue engineered cartilage constructs were

significantly negatively correlated with the passage number of the MSCs used for tissue engineering (**Figures 3E and 3F**)

MSCs were also tested for their osteogenic potential in monolayer culture by semi-quantitative analysis of the staining for alizarin red. Typical images of the staining patterns and the scoring systems used are shown in **Figures S1**. There was some evidence of a gradual loss of osteogenic potency of MSCs however the results were inconsistent between patients. For Patient PN241 there was no apparent change in the mean osteogenic score with cumulative population doublings (**Figure S2A**). For Patient PN242 there was a significant fall in osteogenic potential with cumulative population doublings (**Figures S2B**). PN251 osteogenic scores had already declined to 0 by ten population doublings and remained at 0 for higher doublings, although the change was not statistically significant (**Figure S2C**). Patient PN264 exhibited no observable osteogenic activity even at the earliest number of population doublings (**Figure S2D**). Overall, the individual osteogenic scores for the repeated assays were not significantly correlated with the passage number of the MSCs used (**Figure S2E**), however the different patterns observed with each of the patients are indicative of a gradual, if variable decline in osteogenesis with *in vitro* ageing of the cells.

The adipogenic potential of MSCs was tested in monolayer culture by semi-quantitative analysis of the staining for Oil-Red-O. Typical images of the staining patterns and the scoring systems used are shown in **Figures S3**. For Patient PN251 there was a small but significant fall in adipogenic potential with cumulative population doublings (**Figure S4C**). whereas there was no significant change for the other three patients (**Figures S4A, S4B and S4C**). Overall, the individual adipogenic scores for the repeated assays were not significantly

correlated with the passage number of the MSCs used (**Figure S4E**) and therefore only very limited evidence for a fall in adipogenesis with *in vitro* ageing of the cells.

Collectively, these data indicate a clear loss of differentiation potential of MSCs, with early passage cells tending to show full tri-lineage potential and later passage cells tending to retain only adipogenic potential or adipogenic plus osteogenic but not chondrogenic potential. These data suggest that multipotential differentiation is not a fundamental property of CD105+ve, CD90+ve, CD34-ve, CD45-ve MSCs, but rather a feature of freshly isolated MSCs that is lost with cell expansion *in vitro*.

3.3. Trophic repair by MSCs is maintained with increasing passage

We used meniscal cartilage integration an suppression of T-cell proliferation as assays relating to different aspects of trophic repair.

The *in vitro* integration of two pieces of meniscal cartilage by MSCs was based on our previous studies of this system *in vitro*, in an *in vivo* sheep model and in patients with torn meniscus [27]. MSCs from all four patients at each of 17 passages were tested for their potency in our meniscal repair potency assay. The variation in % integration of meniscus in these studies was in the same range as previously described, as illustrated in typical histological images (**Figures 4A-C**). In contrast to our observations of tri-potential differentiation (see above), there was no significant change in the mean potency of meniscal repair with cumulative population doublings for any of the four patients (**Figures 4D-G**).

Furthermore, the % integration measured for the individual meniscal constructs showed no correlation with the passage number of the MSCs used (**Figure 4H**)

As well as stimulating tissue repair responses, MSCs are also able to suppress immunity through inhibition of T-Cell proliferation and other mechanisms. We therefore measured the % inhibition of T-cell proliferation by MSCs from selected passages for all four patients. As with meniscal repair, there was no significant change in the immunoregulatory capacity of MSCs with increasing passage (**Figure 4I**).

Taken together our observations of trophic repair indicate that the protective and reparative effects of MSCs are a fundamental feature of CD105+ve, CD90+ve, CD34-ve, CD45-ve MSCs, that is retained even after extensive expansion *in vitro*.

Transcriptomics and proteomics data show significant differences over passage that can be linked to loss of multipotency

We reserved mRNA from the undifferentiated MSCs of all four patients at each passage. Based on growth and differentiation characteristics we selected mRNA from passages P1, P5, P10 and P15 for gene array comparison. For each of these passages we also collected conditioned medium for proteomic comparison. The genomic and proteomic data were combined and analysed for patterns of change in related genes and proteins. The methodological approach to transcriptomic and proteomic analysis is illustrated in **Figure 5A**. Data structure was appraised via principal component analysis (PCA). A score plot of the first two principal components is shown in **Figure 5B**. The changes captured over passage

are accounted for in PC2 whilst PC1 captures considerable variation between patients which can be stratified in two groups (shown with blue and orange ellipses). These two groups of patients also show differences in osteogenic capabilities (see above). With the aim of identifying genes and proteins changing solely over passage, independently of this patient variability, we performed a 2-way ANOVA for each variable, as described in the methods section. **Figure 5C** shows the significant variables of these tests. Only 338 genes and proteins are significant uniquely over passage, independently of patient to patient variation or any related iteration. These 338 genes and proteins were used to calculate PCA, of which the first two principal components are shown in **Figure 5D** together with a heatmap of the 338 variables selected. As expected, these genes and proteins show a very clear separation of all the patient samples by passage with a subset decreasing their expression/abundance over passage (top half of the heatmap) while others increase their expression/abundance (bottom half of the heatmap).

For each of these 338 significant proteins and genes we calculated the fold change with respect to passage 1 and analysed these data with Ingenuity Pathway Analysis (IPA) (QIAGEN Inc, https://www.qiagenbioinformatics.com/products/ingenuity-pathway-analysis). IPA's core analysis, overlaid with the global molecular network within the software resulted in the identification of a number of canonical pathways, functions and upstream regulators found to be significantly over-represented within this list and therefore linked to the loss of multipotenial differentiation capacity of the cells. The largest and most significant change was in the cell-cycle master regulator FOXM1 gene pathway, with clear evidence from transcriptomic data for downregulation of the FOXM1 gene itself (**Figure 6A**) and with six out of seven of its downstream effectors also predicted by IPA to be

downregulated (**Figure 6B**). Other upstream regulators predicted to be deactivated were the prostaglandin receptor PTGER2, and members of the VEGF family, whilst upstream regulators that were also predicted to be positively activated over passage included the proliferation regulator NUPR and the cytoskeleton regulator MYOC. Quantitative data from our transcriptomic analyses and the associated IPA predictions of changes in the downstream effectors of these regulators, are shown in **Figure S5**, however none of the changes and predicted downstream effects were as clear-cut as for FOXM1.

3.4. Regulators of cell migration and wound healing can be linked to the trophic properties of MSCs

As shown in Figure 4, the trophic repair capacity of MSCs remains unchanged with increasing passage. With the aim of further investigating this phenomenon we hypothesised that (a) the proteins and genes involved in regulating this function would not present a significant change in abundance/expression over passage and (b) functions related to cell movement, cell migration and wound healing are likely to be mechanistically involved in trophic repair. To investigate this hypothesis, we used the IPA database to identify the proteins and genes involved within the three terms listed above. Then we mapped those lists to our data, extracted overlapping variables and appraised their significance over passage. The large majority of the proteins and genes mapping to these search-terms were found to be unchanged over passage and expressed at a consistent level across all four passages of our MSC cultures (**Figure 6B**), supporting the hypothesis that genes and proteins expected to be necessary for trophic repair continue to be expressed in ageing cells, when multi-potent differentiation capacity has been lost but trophic repair capacity remains high.

We considered CXCL12 (also called Stromal cell-derived factor 1) to be of particular importance at it is associated with all three of our search terms (**Figure 6C**) and was expressed consistently highly at both gene and protein level (**Figures 6D and E**).

3.5. **Marker genes and proteins**

The IPA analysis outlined above demonstrated downregulation of the FOXM1 canonical pathway with increasing passage/loss of multi-potent differentiation and continuous expression of CXCL12 and other cell migration and wound healing genes and proteins with increasing passage. However, we consider it necessary also to identify genes and proteins that may not be part of canonical pathways or gene/protein families, but that can be used as specific markers of cellular ageing *in vitro*. Such markers would aid in comparison of studies of cells from one laboratory to another or in determining the functionality of an MSC population being used for therapeutic purposes. We therefore analysed the gene array and protein data to identify candidate markers.

Within the significant variable genes identified by transcriptomic analysis, there was a significant decrease with increasing passage in the gene for matrix metalloproteinase 13 (MMP13; Collagenase 3; **Figure 7A** and **Table S2**) and a significant increase with increasing passage in the gene for Insulin-like growth factor binding protein 5 (IGF Binding protein 5; **Table S2**). There was no significant change in other MMP genes (**Table S2**) or IGFBP genes (**Table S3**), nor in any of the genes of the Transforming Growth Factor family (**Table S4**). Because the transcriptomic data indicated that the rate of fall in MMP13 gene expression with passage mirrored closely the fall in chondrogenic potential (compare **Figure 7A** with

Figure 3), we went on to validate these results using quantitative PCR to determine more accurately the changes in MMP13 gene expression with increasing passage. The results confirm a continuous decline in MMP13 gene expression with increasing passage (**Figure 7B**), demonstrating that loss of MMP13 gene expression could be used to help determine the extent to which MSCs have aged through *in vitro* proliferation.

Within the proteomic dataset we identified those proteins expressed at highest abundance at all passages (**Table S5**). The most abundant of these proteins was Metalloproteinase Inhibitor 1 (Tissue Inhibitor of Metalloproteinase 1; TIMP1; **Table S5 and Figure 7C**). We went on to validate these results using an ELISA kit assay to determine more accurately the changes in TIMP-1 protein secretion with increasing passage (**Figure 7D**), demonstrating that expression of TIMP-1 is a defining characteristic of MSCs, irrespective of the extent to which they have aged through *in vitro* proliferation. Furthermore, when MSCs were seeded onto collagen scaffolds and cultured for 24h, the cells continued to secrete high levels of MSCs from the cell/scaffold constructs into their culture medium, however if the constructs were freeze-thawed under conditions that reduced their viability, the secreted TIMP levels were substantially reduced (**Figure 7E**).

These results indicate that MMP13^{+}, TIMP1-secreting^{high} MSCs can be used as the basis of injectable therapies for OA that are intended to act primarily through engraftment and chondrogneic differentiation. In contrast, MMP13^{-}, TIMP1-secreting^{high} MSCs can be used for OA therapies that are intended to act primarily through trophic repair.

4. DISCUSSION

We have identified two functional markers relating to MSC ageing *in vitro*, namely the MMP13 (Collagenase 3) gene, which is downregulated with increasing passage, and TIMP-1 protein, which is the most abundant protein in the secretome at all passages. It is particularly interesting that these two markers, which were identified independently of each other (one from transcriptomics data and one form proteomics), are biologically related to each other as TIMP-1 is an inhibitor of MMP13 as well as other metalloproteinases. This relationship is important because it could explain how production of a catabolic proteinase (MMP13) correlates to an anabolic capacity of MSCs (chondrogenesis). The very high levels of TIMP-1 produced by undifferentiated MSCs at all passages will most likely inhibit the any activated MMP13 rendering it catabolically inert. In an OA cell therapy context, TIMP-1 protein secretion could be used as a specific marker of MSC identity and viability as it is constitutively expressed at very high levels at all passages whether growing on tissue culture plastic or seeded into three-dimensional scaffolds. MMP13 gene expression could be used as a functional marker to distinguish chondrogenic MSCs from those that have good trophic capacity but poor chondrogenic capacity.

These results also have important implications for the strategies that should be employed in the development of injectable OA therapies. Since MMP13^{+}, TIMP1-secreting^{high} MSCs were lost as early as passage 5, it seems likely that OA therapies that are intended to act through engraftment and chondrogenic differentiation will be restricted to the use of autologous cells, because viable allogenic products would require far more extensive expansion. Whilst we cannot rule out the possibility that alternative culture condition to those used here could be identified as a method of sustaining the chondrogenic phenotype even after *in*

vitro ageing, the present data nevertheless lead us to conclude that allogeneic injectable stem cell therapies for OA should rather focus on the use of MMP13^{-}, TIMP1-secreting^{high} MSCs acting through trophic repair mechanisms.

Our results also have important biological implications. They clearly indicate that the loss of multipotent differentiation capacity of MSCs with extensive passaging *in vitro* cannot be the result of a generalised loss of cell function as the MSCs senesce, since another important property of MSCs, trophic repair, is not significantly reduced even after a very high number of population doublings and reduced chondrogenic differentiation capacity was observed many passages before cessation of proliferation. Furthermore, families of genes and proteins from a range of critical signalling pathways show clear changes that correlate with increasing passage number and loss of differentiation, whereas genes and proteins known to be involved with wound repair and cell movement/migration do not vary significantly with increasing passage number. Downregulation of the Forkhead Box M1 (FOXM1) canonical pathway showed a clear relationship to passage number, indicating a potential role for FOXM1 in the maintenance and then loss of multipotency. This observation is consistent with previous studies of its biological function. It is a proto-oncogene that is a key master regulator in the survival of cancer stem cells [49, 50]. It has also been shown to be highly expressed in multipotent and pluripotent stem cells and to be critical to the maintenance of stem cell potency [51, 52] and to the induction of pluripotency through reprogramming [53]. CXCL12 (also known as SDF-1) was found to be associated with all three of our search terms related to trophic repair and its gene and protein levels were maintained even at very late passage numbers, indicating a potential role for CXCL12 in MSC-mediated trophic repair. This observation is consistent with previous studies which

have demonstrated its critical role in MSC-mediated induction of spinal cord repair [54] and myocardial repair [55], as well as enhancing nerve cell survival *in vitro* [56] and mediating trophism between endothelial cells and tumour cells [57]. We have identified FOXM1 and CXCL12 through combined proteomic and genomic analysis, but whilst this *in silico* approach is a powerful tool, any mechanistic involvement of these regulators must await experimental confirmation.

Previous studies have clearly shown that multipotency of MSCs declines with both *in vitro* and *in vivo* ageing [33-39]. Our observation here that chondrogenesis declines, osteogenesis tends to decline, but adipogenesis is retained at higher passage number is in agreement with the work of Yang et al [34]. Muraglia et al [36] also showed a loss of multipotent differentiation with passage, but in their experiments, osteogenesis was retained with early loss of adipogenesis. However, they were working with clonal MSC cell-lines whereas the work reported here and by Yang et al investigated the whole MSC population.

Haynesworth et al first described the unique cytokine expression pattern of MSCs [58] and they demonstrated a reduction in cytokine production after stimulating differentiation using dexamethasone. A decade later, Caplan and Dennis coined the term "trophic effect" which they defined as "those chemotactic, mitotic, and differentiation-modulating effects which emanate from cells as bioactive factors that exert their effects primarily on neighbouring cells and whose effects never result in differentiation of the producer cell" [22]. They cited, as a typical example of this effect, the support provided by MSCs in the bone marrow niche for growth and differentiation of haematopoetic cells. They also summarised evidence for

MSCs providing trophic support in a range of cell therapy settings including the treatment of stroke, myocardial infarction and meniscal cartilage regeneration. Numerous other studies have gone on to describe the importance of MSC-induced trophic repair [20, 22-25]. We exploited the trophic effects of MSCs in devising a new method of treating fresh meniscal cartilage tears using a stem cell/collagen-scaffold implant to promote integration of the damaged tissue. Our original *in vitro* studies demonstrated that the method depends on cell migration from the implant into surrounding tissue and interaction with the endogenous meniscal cells [26, 46]. Importantly, we found that MSCs that have been stimulated with Transforming Growth Factor ß to undergo chondrogenic differentiation are much less potent at promoting meniscal repair than the undifferentiated MSCs [26]. We went on to describe the use of undifferentiated MSCs seeded on a collagen scaffold to repair meniscal injury in a sheep pre-clinical model and in a first in human trial [27]. In the current study we used our *in vitro* semi-quantitative meniscal cartilage integration assay [26] as a model for trophic repair and made the very surprising observation that MSCs that have been cultured for up to 30 passages retain the same capacity for trophic repair as very early passage cells. These functional data were supported by our analysis of genes and proteins involved with cell movement and migration and with wound healing, showing that unlike those linked to differentiation, there was no significant change in their expression with increasing passage.

Another aspect of MSC trophism is the immunoregulatory effects of MSCs. Although a range of mechanisms are involved, it is clear that inhibition of T-cell proliferation is a critical component of their suppressive activity [9, 24, 28-31]. Human T-cells can be strongly stimulated to proliferate using a combination of anti-CD3 and anti-CD28 antibodies [59].

Their rate of proliferation can be monitored by covalently labelling intracellular molecules with a fluorescent dye that is then diluted out by 50% with each cell division, tracked by FACS [60]. Adding MSCs into cultures of labelled, stimulated T-cells suppresses the lymphocyte proliferation, so prolonging the accumulation of the dye [9]. In the current study, we have used this method to measure the immunoregulatory effects of MSCs at early and late passage and found no loss of potency with increasing passage. For human MSCs, the mechanism of T-cell suppression has been described as involving indoleamine 2,3-dioxygenase-mediated tryptophan degradation [61]. Taken together, these results demonstrate that, as with trophic repair, immunoregulation is a fundamental property of MSCs that is not lost with increasing passage.

Previous studies have proposed that the loss of multipotent differentiation capacity of MSCs with increasing passage is related to progression of the cells to a senescent end-state [33-36]. However, the results described here demonstrate that even after extensive passaging *in vitro*, there is no apparent loss of trophic repair. The term "Mesenchymal Stem Cells" was coined by Caplan [1], who went on to describe MSCs as "An injury Drugstore" [23] and more recently advocated a change in their name to "Medicinal Signaling Cells" [62]. Other studies have questioned the definition of MSCs as stem cells because of the lack of rigorous confirmatory biological evidence [20, 25, 31, 63, 64], with all of these studies calling for more experimental data before reaching a conclusion on the nomenclature. Others have been more forthright in concluding that MSCs are not stem cells and have called for an immediate change in nomenclature, in order to avoid the over-hyped marketing of MSCs as "miracle cures" [65-67]. Prockop emphasised that the essence of a stem cell should not be determined by its status at a single point in time [25]. In this study, we have investigated

the *in vitro* differentiation and trophic behaviour of MSCs across many passages over time and in this way, have reached the conclusion that the property of multipotency is relatively transient whereas the trophic effects of these cells is apparently permanent all the way through to the time of growth arrest.

5. Conclusion

These studies demonstrate that the development of injectable MSC therapies for OA must take into account the transient nature of chondrogenic potency relative to their sustained trophic potency with increasing passage and specific strategies should be adopted to exploit one or other of these mechanisms of action.

ACKNOWLEDGEMENTS

This work was supported by a grant from Innovate UK [grant number: 102164]. M.R. was funded by an Erasmus+ Traineeship mobility grant [student number: 3930572].

The work was also supported by the NIHR Biomedical Research Centre at University Hospitals Bristol NHS Foundation Trust and the University of Bristol. The views expressed in this publication are those of the author(s) and not necessarily those of the NHS, the National Institute for Health Research or the Department of Health and Social Care.

CONFLICTS OF INTERESTS

The work reported here was part of a larger project funded by Innovate UK and led by Azellon Ltd, a spin-out company from University of Bristol, UK. A.P.H. is a founder and share-holder in Azellon Ltd. Some of the findings reported here are the subject of a patent filing by The University of Liverpool.

DATA AVAILABILITY STATEMENT

The data that support the findings of this study are available from the corresponding author upon reasonable request.

REFERENCES

1. Caplan AI. Mesenchymal stem cells. **J Orthop Res***.* 1991;9:641-650.
2. Friedenstein AJ, Piatetzky S, II, Petrakova KV. Osteogenesis in transplants of bone marrow cells. **J Embryol Exp Morphol***.* 1966;16:381-390.
3. Friedenstein AJ, Petrakova KV, Kurolesova AI et al. Heterotopic of bone marrow.Analysis of precursor cells for osteogenic and hematopoietic tissues. **Transplantation***.* 1968;6:230-247.
4. Friedenstein AJ, Chailakhjan RK, Lalykina KS. The development of fibroblast colonies in monolayer cultures of guinea-pig bone marrow and spleen cells. **Cell Tissue Kinet***.* 1970;3:393-403.
5. Kolf CM, Cho E, Tuan RS. Mesenchymal stromal cells. Biology of adult mesenchymal stem cells: regulation of niche, self-renewal and differentiation. **Arthritis Res Ther***.* 2007;9:204.
6. Kafienah W, Mistry S, Williams C et al. Nucleostemin is a marker of proliferating stromal stem cells in adult human bone marrow. **Stem Cells***.* 2006;24:1113-1120.
7. Kafienah W, Jakob M, Demarteau O et al. Three dimensional tissue engineering of hyaline cartilage: comparison of adult nasal and articular chondrocytes. **Tissue Engineering***.* 2002;8:817-826.
8. Kafienah W, Mistry S, Perry MJ et al. Pharmacological Regulation of Adult Stem Cells: Chondrogenesis can be Induced Using A Synthetic Inhibitor of the Retinoic Acid Receptor. **Stem Cells***.* 2007;25:2460-2468.
9. Dickinson SC, Sutton CA, Brady K et al. The Wnt5a Receptor, Receptor Tyrosine Kinase-Like Orphan Receptor 2, Is a Predictive Cell Surface Marker of Human Mesenchymal Stem Cells with an Enhanced Capacity for Chondrogenic Differentiation. **Stem Cells***.* 2017;35:2280-2291.
10. Yoo JU, Barthel TS, Nishimura K et al. The chondrogenic potential of human bone-marrow-derived mesenchymal progenitor cells. **J Bone Joint Surg Am***.* 1998;80:1745-1757.
11. Johnstone B, Hering TM, Caplan AI et al. In vitro chondrogenesis of bone marrow-derived mesenchymal progenitor cells. **Exp Cell Res***.* 1998;238:265-272.
12. Solchaga LA, Penick K, Porter JD et al. FGF-2 enhances the mitotic and chondrogenic potentials of human adult bone marrow-derived mesenchymal stem cells. **J Cell Physiol***.* 2005;203:398-409.
13. Martin I, Muraglia A, Campanile G et al. Fibroblast growth factor-2 supports ex vivo expansion and maintenance of osteogenic precursors from human bone marrow. **Endocrinology***.* 1997;138:4456-4462.
14. Gronthos S, Graves SE, Ohta S et al. The STRO-1+ fraction of adult human bone marrow contains the osteogenic precursors. **Blood***.* 1994;84:4164-4173.
15. Pound JC, Green DW, Roach HI et al. An ex vivo model for chondrogenesis and osteogenesis. **Biomaterials***.* 2007;28:2839-2849.
16. Pound JC, Green DW, Chaudhuri JB et al. Strategies to promote chondrogenesis and osteogenesis from human bone marrow cells and articular chondrocytes encapsulated in polysaccharide templates. **Tissue Eng***.* 2006;12:2789-2799.
17. Simonsen JL, Rosada C, Serakinci N et al. Telomerase expression extends the proliferative life-span and maintains the osteogenic potential of human bone marrow stromal cells. **Nat Biotechnol***.* 2002;20:592-596.

18. Mirmalek-Sani SH, Tare RS, Morgan SM et al. Characterization and multipotentiality of human fetal femur-derived cells: implications for skeletal tissue regeneration. **Stem Cells**. 2006;24:1042-1053.
19. Munir H, Ward LSC, Sheriff L et al. Adipogenic Differentiation of Mesenchymal Stem Cells Alters Their Immunomodulatory Properties in a Tissue-Specific Manner. **Stem Cells**. 2017;35:1636-1646.
20. Kuroda Y, Kitada M, Wakao S et al. Bone Marrow Mesenchymal Cells: How Do They Contribute to Tissue Repair and Are They Really Stem Cells? **Archivum immunologiae et therapiae experimentalis**. 2011.
21. Prockop DJ. "Stemness" does not explain the repair of many tissues by mesenchymal stem/multipotent stromal cells (MSCs). **Clin Pharmacol Ther**. 2007;82:241-243.
22. Caplan AI, Dennis JE. Mesenchymal stem cells as trophic mediators. **J Cell Biochem**. 2006;98:1076-1084.
23. Caplan AI, Correa D. The MSC: an injury drugstore. **Cell Stem Cell**. 2011;9:11-15.
24. Tolar J, Le Blanc K, Keating A et al. Concise review: hitting the right spot with mesenchymal stromal cells. **Stem Cells**. 2010;28:1446-1455.
25. Prockop DJ. Repair of tissues by adult stem/progenitor cells (MSCs): controversies, myths, and changing paradigms. **Mol Ther**. 2009;17:939-946.
26. Pabbruwe MB, Kafienah W, Tarlton JF et al. Repair of meniscal cartilage white zone tears using a stem cell/collagen-scaffold implant. **Biomaterials**. 2010;31:2583-2591.
27. Whitehouse MR, Howells NR, Parry MC et al. Repair of Torn Avascular Meniscal Cartilage Using Undifferentiated Autologous Mesenchymal Stem Cells: From In Vitro Optimization to a First-in-Human Study. **Stem Cells Transl Med**. 2017;6:1237-1248.
28. Uccelli A, Pistoia V, Moretta L. Mesenchymal stem cells: a new strategy for immunosuppression? **Trends Immunol**. 2007;28:219-226.
29. Uccelli A, Moretta L, Pistoia V. Immunoregulatory function of mesenchymal stem cells. **European Journal of Immunology**. 2006;36:2566-2573.
30. Spaggiari GM, Capobianco A, Abdelrazik H et al. Mesenchymal stem cells inhibit natural killer cell proliferation, cytotoxicity and cytokine production: role of indoleamine 2,3-dioxygenase and prostaglandin E2. **Blood**. 2007.
31. Keating A. Mesenchymal stromal cells: new directions. **Cell stem cell**. 2012;10:709-716.
32. Lazarus HM, Koc ON, Devine SM et al. Cotransplantation of HLA-identical sibling culture-expanded mesenchymal stem cells and hematopoietic stem cells in hematologic malignancy patients. **Biol Blood Marrow Transplant**. 2005;11:389-398.
33. Yang YK. Aging of mesenchymal stem cells: Implication in regenerative medicine. **Regen Ther**. 2018;9:120-122.
34. Yang YK, Ogando CR, Wang See C et al. Changes in phenotype and differentiation potential of human mesenchymal stem cells aging in vitro. **Stem Cell Res Ther**. 2018;9:131.
35. Bonab MM, Alimoghaddam K, Talebian F et al. Aging of mesenchymal stem cell in vitro. **BMC Cell Biol**. 2006;7:14.
36. Muraglia A, Cancedda R, Quarto R. Clonal mesenchymal progenitors from human bone marrow differentiate in vitro according to a hierarchical model. **J Cell Sci**. 2000;113 (Pt 7):1161-1166.

37. Ganguly P, El-Jawhari JJ, Giannoudis PV et al. Age-related Changes in Bone Marrow Mesenchymal Stromal Cells: A Potential Impact on Osteoporosis and Osteoarthritis Development. **Cell Transplant**. 2017;26:1520-1529.
38. Choudhery MS, Badowski M, Muise A et al. Donor age negatively impacts adipose tissue-derived mesenchymal stem cell expansion and differentiation. **J Transl Med**. 2014;12:8.
39. Stenderup K, Justesen J, Clausen C et al. Aging is associated with decreased maximal life span and accelerated senescence of bone marrow stromal cells. **Bone**. 2003;33:919-926.
40. Baxter MA, Wynn RF, Jowitt SN et al. Study of telomere length reveals rapid aging of human marrow stromal cells following in vitro expansion. **Stem Cells**. 2004;22:675-682.
41. Kafienah W, Mistry S, Dickinson S et al. Three-dimensional cartilage tissue engineering using adult stem cells from osteoarthritis patients. **Arthritis Rheum**. 2007;56:177-187.
42. Bianchi G, Banfi A, Mastrogiacomo M et al. Ex vivo enrichment of mesenchymal cell progenitors by fibroblast growth factor 2. **Exp Cell Res**. 2003;287:98-105.
43. Martin I, Vunjak-Novakovic G, Yang J et al. Mammalian chondrocytes expanded in the presence of fibroblast growth factor 2 maintain the ability to differentiate and regenerate three- dimensional cartilaginous tissue. **Exp Cell Res**. 1999;253:681-688.
44. Dickinson SC, Sims TJ, Pittarello L et al. Quantitative outcome measures of cartilage repair in patients treated by tissue engineering. **Tissue Eng**. 2005;11:277-287.
45. Handley CJ, Buttle DJ. Assay of proteoglycan degradation. **Methods Enzymol**. 1995;248:47-58.
46. Pabbruwe MB, Esfandiari E, Kafienah W et al. Induction of cartilage integration by a chondrocyte/collagen-scaffold implant. **Biomaterials**. 2009;30:4277-4286.
47. Pabbruwe MB, Kafienah W, Tarlton JF et al. Repair of meniscal cartilage white zone tears using a stem cell/collagen-scaffold implant. **Biomaterials**. 2010;31:2583-2591.
48. Langdon WB. Performance of genetic programming optimised Bowtie2 on genome comparison and analytic testing (GCAT) benchmarks. **BioData Min**. 2015;8:1.
49. Nakano I. Transcription factors as master regulator for cancer stemness: remove milk from fox? **Expert Rev Anticancer Ther**. 2014;14:873-875.
50. Xie Z, Tan G, Ding M et al. Foxm1 transcription factor is required for maintenance of pluripotency of P19 embryonal carcinoma cells. **Nucleic Acids Res**. 2010;38:8027-8038.
51. Besharat ZM, Abballe L, Cicconardi F et al. Foxm1 controls a pro-stemness microRNA network in neural stem cells. **Sci Rep**. 2018;8:3523.
52. Youn M, Wang N, LaVasseur C et al. Loss of Forkhead box M1 promotes erythropoiesis through increased proliferation of erythroid progenitors. **Haematologica**. 2017;102:826-834.
53. Jeong HS, Bhin J, Joon Kim H et al. Transcriptional regulatory networks underlying the reprogramming of spermatogonial stem cells to multipotent stem cells. **Exp Mol Med**. 2017;49:e315.
54. Stewart AN, Matyas JJ, Welchko RM et al. SDF-1 overexpression by mesenchymal stem cells enhances GAP-43-positive axonal growth following spinal cord injury. **Restor Neurol Neurosci**. 2017;35:395-411.

55. Dong F, Harvey J, Finan A et al. Myocardial CXCR4 expression is required for mesenchymal stem cell mediated repair following acute myocardial infarction. **Circulation**. 2012;126:314-324.
56. Chalasani SH, Baribaud F, Coughlan CM et al. The chemokine stromal cell-derived factor-1 promotes the survival of embryonic retinal ganglion cells. **J Neurosci**. 2003;23:4601-4612.
57. Rao S, Sengupta R, Choe EJ et al. CXCL12 mediates trophic interactions between endothelial and tumor cells in glioblastoma. **PLoS One**. 2012;7:e33005.
58. Haynesworth SE, Baber MA, Caplan AI. Cytokine expression by human marrow-derived mesenchymal progenitor cells in vitro: effects of dexamethasone and IL-1 alpha. **J Cell Physiol**. 1996;166:585-592.
59. Verhagen J, Wraith DC. Blockade of LFA-1 augments in vitro differentiation of antigen-induced Foxp3(+) Treg cells. **J Immunol Methods**. 2014;414:58-64.
60. Quah BJ, Warren HS, Parish CR. Monitoring lymphocyte proliferation in vitro and in vivo with the intracellular fluorescent dye carboxyfluorescein diacetate succinimidyl ester. **Nat Protoc**. 2007;2:2049-2056.
61. Meisel R, Zibert A, Laryea M et al. Human bone marrow stromal cells inhibit allogeneic T-cell responses by indoleamine 2,3-dioxygenase-mediated tryptophan degradation. **Blood**. 2004;103:4619-4621.
62. Caplan AI. Mesenchymal Stem Cells: Time to Change the Name! **Stem Cells Transl Med**. 2017;6:1445-1451.
63. Javazon EH, Beggs KJ, Flake AW. Mesenchymal stem cells: paradoxes of passaging. **Experimental hematology**. 2004;32:414-425.
64. Bianco P, Robey PG, Simmons PJ. Mesenchymal stem cells: revisiting history, concepts, and assays. **Cell Stem Cell**. 2008;2:313-319.
65. Sipp D, Robey PG, Turner L. Clear up this stem-cell mess. **Nature**. 2018;561:455-457.
66. Caulfield T, Sipp D, Murry CE et al. SCIENTIFIC COMMUNITY. Confronting stem cell hype. **Science**. 2016;352:776-777.
67. Sipp D, Caulfield T, Kaye J et al. Marketing of unproven stem cell-based interventions: A call to action. **Sci Transl Med**. 2017;9.

FIGURE LEGENDS

Figure 1. Growth and phenotypic characteristics of MSCs from four patients

(A) The number of population doublings reached after each passage using MSCs from each patient were recorded until growth ceased (for PN242 data were collected until passage 30, when the cells continued to grow). (B) The population doubling time is shown up to passage 17 for all four patients. (C) Typical cell morphology is shown for PN251 MSCs at passage 4 and passage 16 (growth arrest was at passage 17 for this patient) and for PN242 at passage 19 (no growth arrest observed for this patient). Size bars = 200μM. (D) The percentage of cells expressing MSC markers CD90 and CD105 and haematopoietic stem cell markers CD34 and CD45 were determined by Fluorescence Activated Cell Sorting.

Figure 2. Macroscopic appearance of tissue engineered cartilage made using MSCs from four patients at multiple passages

MSCs from passages 2-16 were seeded onto polyglycolic acid scaffolds before being induced to undergo chondrogenic differentiation. Each image shows replicate samples from each patient at each passage that was investigated.

Figure 3. Biochemical properties of tissue engineered cartilage made using MSCs from four patients at multiple passages

MSCs from each patient across a range of passages were used to tissue engineer cartilage, as shown in Figure 2. (A-D) The relationship between dry weight or glycosaminoglycans

(GAG) content of tissue engineered cartilage constructs and the population doublings of MSCs at the time of tissue engineering are shown for each of the patients. For all the graphs, each point shows the mean value of multiple tissue engineering replicates made using cells from one patient at a single passage. (E) The relationship between dry weight of tissue engineered cartilage constructs and the passage number of MSCs at the time of tissue engineering are shown for all four patients. Each point is the result for a single replicate sample. (F) The relationship between the GAG content of tissue engineered cartilage constructs and the passage number of MSCs at the time of tissue engineering are shown for all four patients. Each point is the result for a single replicate sample. For all graphs, the line represents a linear model of degree 1 fitted to the points whilst the spearman rank correlation coefficient and its significance is shown in the top right corner.

Figure 4. Trophic repair of meniscal cartilage and immunoregulation by MSCs from four patients at multiple passages

For trophic repair of meniscal cartilage, undifferentiated MSCs were seeded onto a collagen scaffolds, inserted between two pieces of sheep meniscus, clipped together and cultured for 30 days. Histomorphometry was used to measure the degree of integration between the two pieces of meniscal tissue. (A-C) Typical examples of high, medium and poor integration of meniscal tissue. Integration was measured in between the arrows. Size bars = 1mm. (D-G) The relationship between % integration of meniscal tissue and the population doublings of MSCs are shown for each of the patients. For all the graphs, each point shows the mean value of multiple experimental replicates using cells from one patient at a single passage. (H) The relationship between % integration of meniscal tissue and the passage number of

MSCs are shown for all four patients. Each point is the result for a single replicate sample. For all correlation graphs (A-H), the line represents a linear model of degree 1 fitted to the points whilst the spearman rank correlation coefficient and its significance is shown in the top right corner. (I) Immunoregulation was determined as the % inhibition of T-cell proliferation, measured as the loss of Cell-Trace Violet from labelled cells, quantified by FACS. Each point is the result for pooled triplicate wells.

Figure 5. Transcriptomics and proteomics

(A) Overview of analytical steps performed. Transcriptomics and proteomics data were processed according to data standards and integrated. The integrated data were further analysed by Ingenuity Pathway Analysis to identify key genes and proteins that change over passage and map them to biological functions and predict possible upstream regulators (see **Figures 6 and 7**). (B) Principal Component Analysis (PCA) score plot of first two principal components of all genes and proteins. There is a segregation of patients (see blue and orange ellipses) that can also be linked to changes in osteogenic capabilities (see Figures S2), whilst changes related to passage are capture mainly in PC2. (C) Venn diagram of significant variables after 2-way ANOVA test revealing 338 genes and proteins that vary significantly and independently of the patient group variation. (D) PCA of the 338 significant variables over passage. Shown the score plot of the first 2 principal components (capturing approximately 70% of variance). As expected there is a marked segregation over passage. Heatmap of scaled data from the 338 significant proteins and genes that are represented in rows and clustered via Ward hierarchical clustering. Columns represent biological samples,

each column is a patient sample and they are ordered by passage with red being passage 1, green passage 5, turquoise passage 10 and purple passage 15.

Figure 6. Ingenuity Pathway Analysis of integrated transcriptomics and proteomics data

(A) Ingenuity pathway analysis identified FOXM1 and four other master regulators genes (see **Figure S5**) that vary with increasing passage number. FOXM1 data from transcriptomics analysis shows inhibition of gene expression with increasing passage number. Each bar is the mean ± SEM for results using MSCs from each of the four patients. (B) Ingenuity pathway analysis of the integrated transcriptomics and proteomics data set predicts inhibition of five out of six of the identified downstream regulators in the FOXM1 canonical pathway. (C) Ingenuity pathway analysis identified multiple genes and proteins that mapped to the search terms “Cell Movement”, Cell Migration” or “Wound Healing”. Most of these identified genes and proteins did not vary significantly over passage as determined by ANOVA. The most highly expressed genes and proteins are listed for each of the search terms. (D) CXCL12 data from transcriptomics analysis shows continuous gene expression with increasing passage number. Each bar is the mean ± SEM for results using MSCs from each of the four patients. (E) CXCL12 data from proteomics analysis shows continuous protein secretion with increasing passage number. Each bar is the mean ± SEM for results using MSCs from each of the four patients.

Figure 7. Gene and protein markers of the *in vitro* MSC ageing process

The MMP13 gene was selected as a marker of early passage cells which is lost with ageing of MSCs *in vitro* whilst secretion of the TIMP-1 protein was selected as a marker of MSCs that is independent of *in vitro* ageing. (A) MMP13 data from transcriptomics analysis shows decreasing gene expression with increasing passage number. Each bar is the mean ± SEM for results using MSCs from each of the four patients. (B) MMP13 data from qPCR analysis shows decreasing gene expression with increasing passage number. Each bar is the mean ± SEM for results using MSCs from each of the four patients. (C) TIMP-1 data from proteomics analysis shows continuous protein secretion with increasing passage number. Each bar is the mean ± SEM for results using MSCs from each of the four patients. (D) TIMP-1 data from ELISA analysis shows continuous protein secretion with increasing passage number. Each bar is the mean ± SEM for results using MSCs from each of the four patients. (E) ELISA analysis of TIMP-1 secreted by MSC/collagen scaffold constructs shows continuous protein secretion with increasing passage number for fresh constructs but reduced secretion from constructs that have been freeze-thawed under conditions that reduce their viability. For each cells source the result is shown for one fresh compared with one frozen construct.

Figure S1. Guidance template images for osteogenic scoring

MSCs were induced to undergo osteogenic differentiation and then stained with alizarin red. Each well of the 24-well plate was then scored for mineral deposition (see Figure S2 for results). Typical clusters of positive cells are shown. Each well was graded as being – (see CTL, controls); +; ++; +++ or ++++ by two independent observers. Size bars = 200µM.

Figure S2. Osteogenic differentiation of MSCs from four patients at multiple passages

MSCs from each patient across a range of passages were induced to undergo osteogenic differentiation *in vitro* and scored as shown in Figure S1. (A-D) The relationship between osteogenic score and the cumulative population doublings of MSCs are shown for each of the patients. For all the graphs, each point shows the mean value of multiple replicates using cells from one patient at a single passage. (E) The relationship between the osteogenic score and the passage number of MSCs are shown for all four patients. Each point is the result for a single replicate sample. For all graphs, the line represents a linear model of degree 1 fitted to the points whilst the spearman rank correlation coefficient and its significance is shown in the top right corner.

Figure S3. Guidance template images for adipogenic scoring

MSCs were induced to undergo adipogenic differentiation and then stained with oil red O. Each well of the 24-well plate then was scored for adipogenesis (see Figure S4 for results). Typical clusters of adipogenic cells are shown. Each well was graded as being – (see CTL, controls); +; ++; +++ or ++++ by two independent observers. Size bars = 200µM.

Figure S4. Adipogenic differentiation of MSCs from four patients at multiple passages

MSCs from each patient across a range of passages were induced to undergo adipogenic differentiation *in vitro* and scored as shown in Figure S3. (A-D) The relationship between adipogenic score and the cumulative population doublings of MSCs are shown for each of

the patients. For all the graphs, each point shows the mean value of multiple replicates using cells from one patient at a single passage. (E) The relationship between the adipogenic score and the passage number of MSCs are shown for all four patients. Each point is the result for a single replicate sample. For all graphs, the line represents a linear model of degree 1 fitted to the points whilst the spearman rank correlation coefficient and its significance is shown in the top right corner.

Figure S5. Ingenuity Pathway Analysis of genes and proteins that vary with increasing passage

Ingenuity pathway analysis identified FOXM1 (See **Figure 6**) and four other master regulators genes that vary with increasing passage number. (A) Relationship between MYOC data from transcriptomics analysis and increasing passage number and Ingenuity pathway analysis of the integrated transcriptomics and proteomics data set. Each bar is the mean ± SEM for results using MSCs from each of the four patients. (B) Relationship between NUPR1 data from transcriptomics analysis and increasing passage number and Ingenuity pathway analysis of the integrated transcriptomics and proteomics data set. Each bar is the mean ± SEM for results using MSCs from each of the four patients. (C) Relationship between VEGF data from transcriptomics analysis and increasing passage number and Ingenuity pathway analysis of the integrated transcriptomics and proteomics data set. Each bar is the mean ± SEM for results using MSCs from each of the four patients. (D) Relationship between PTGER2 data from transcriptomics analysis and increasing passage number and Ingenuity pathway analysis of the integrated transcriptomics and proteomics data set. Each bar is the mean ± SEM for results using MSCs from each of the four patients.

Graphical abstract

Ageing of human Mesenchymal stem/stromal cells (MSCs) *in vitro* through prolonged culture and passage results in loss of their chondrogenic potential but no reduction in their trophic repair capacity, allowing the identification of gene and protein markers of these different functions.

TOP

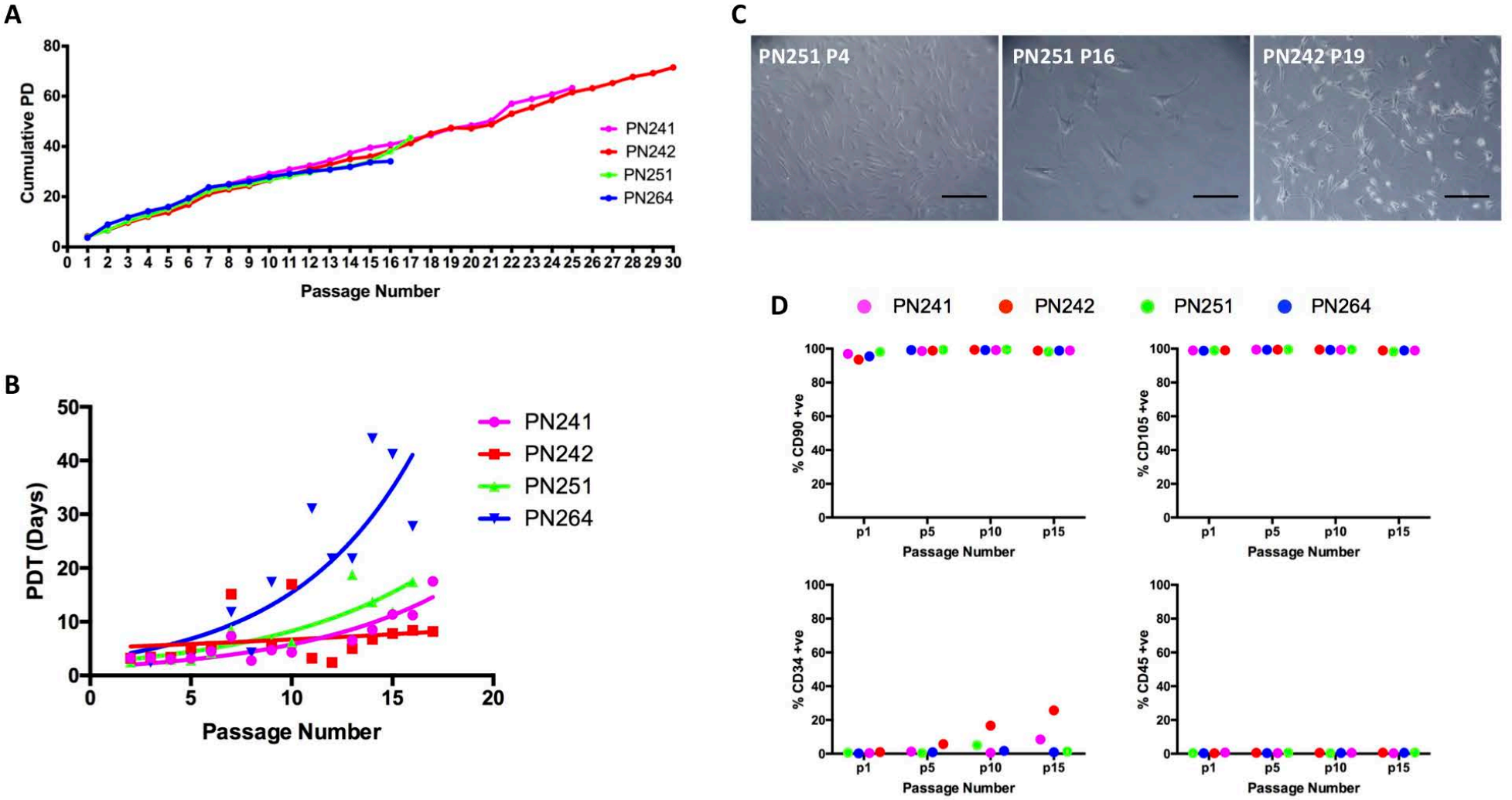

HOLLANDER Figure 1

TOP

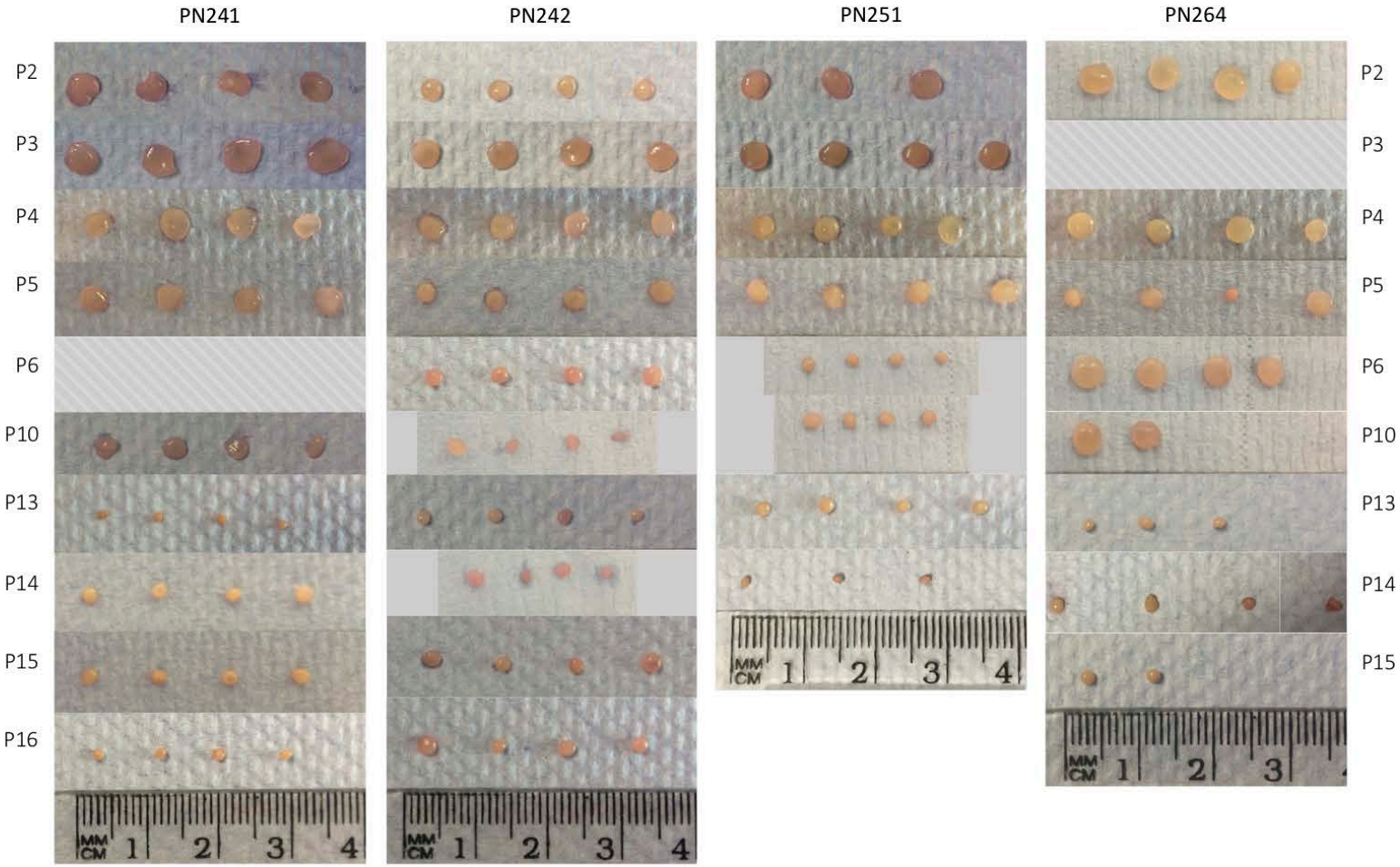

HOLLANDER Figure 2

TOP

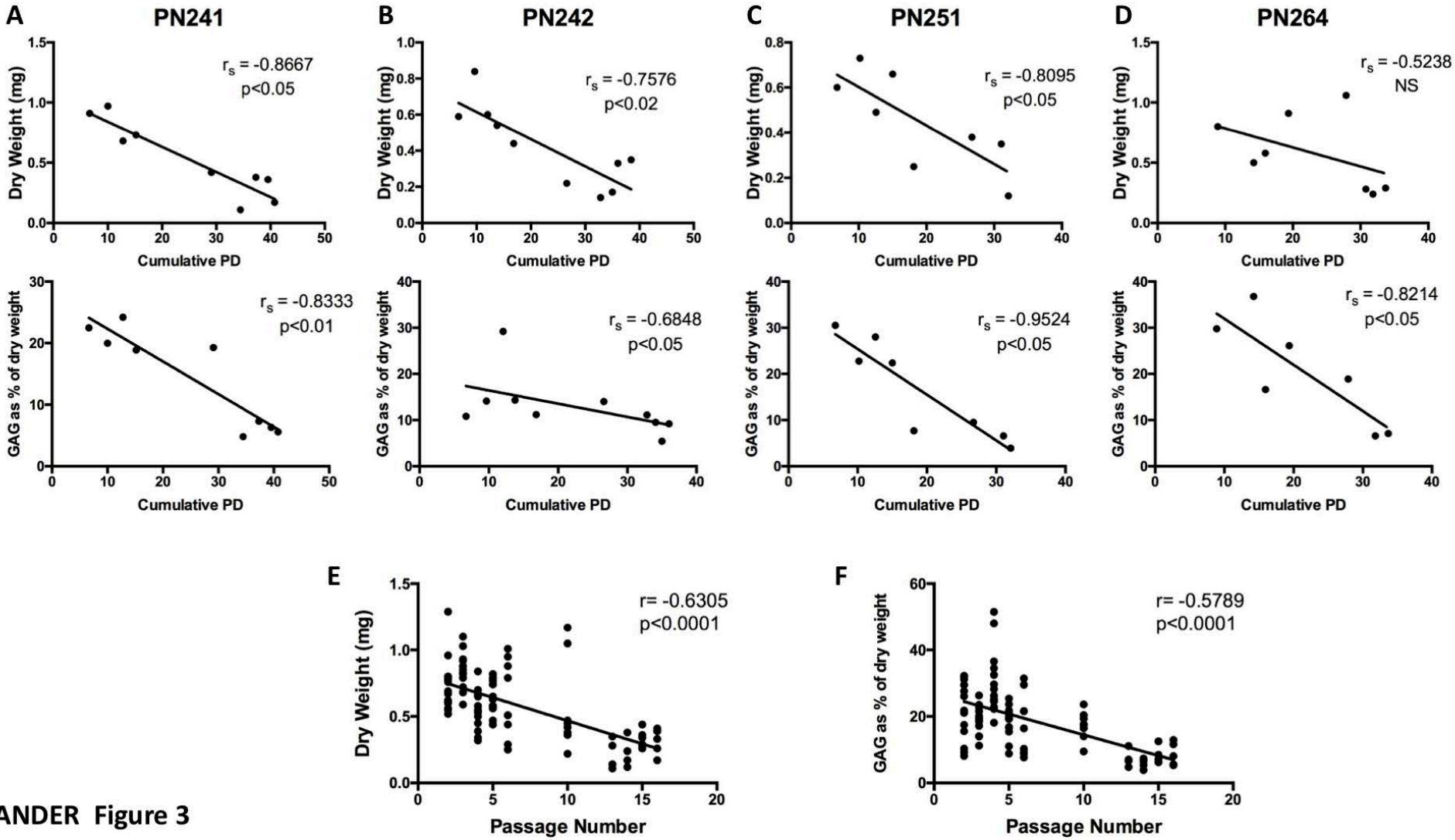

HOLLANDER Figure 3

TOP

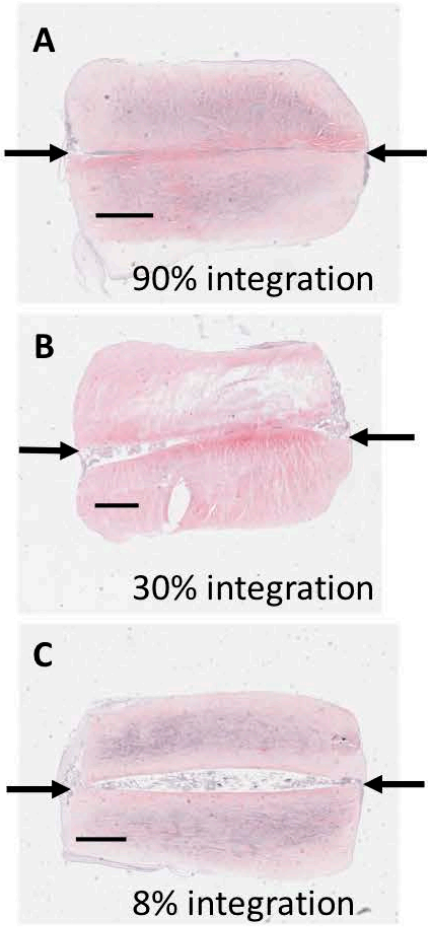

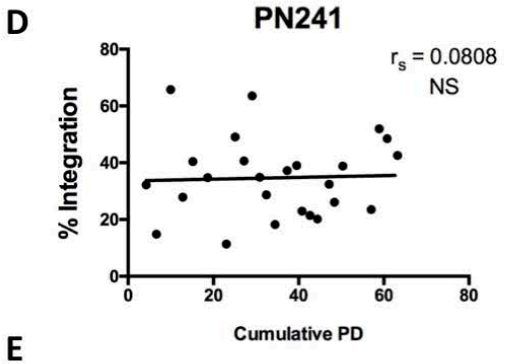

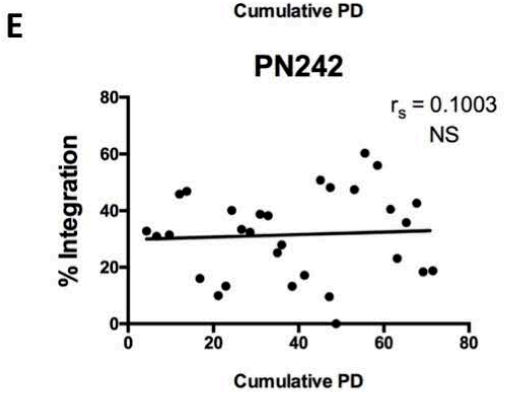

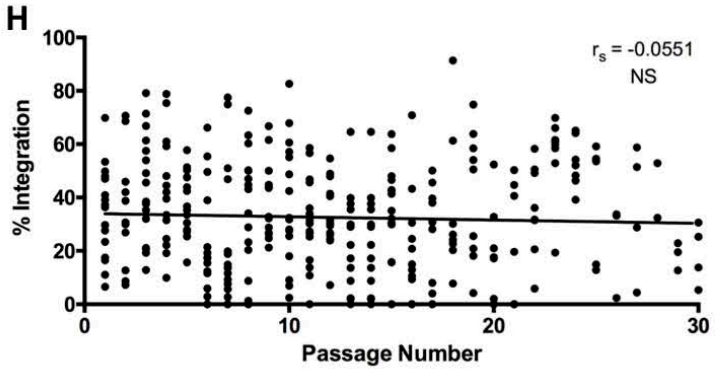

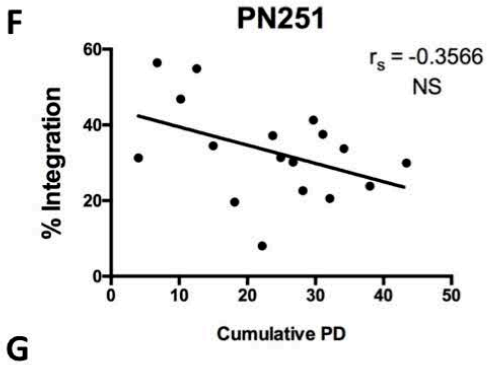

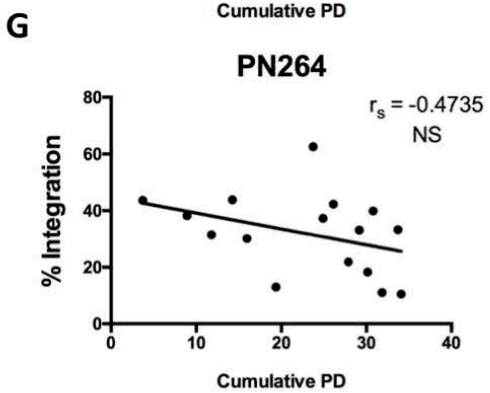

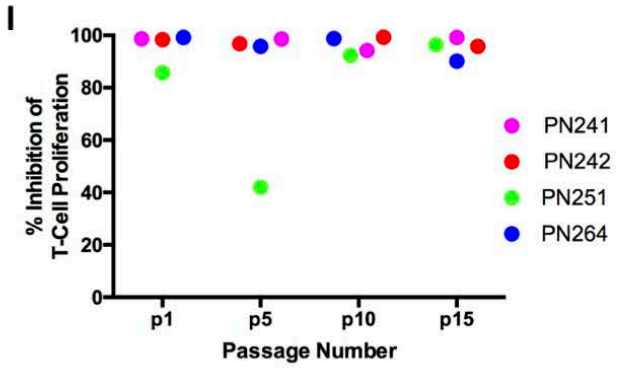

HOLLANDER Figure 4

TOP

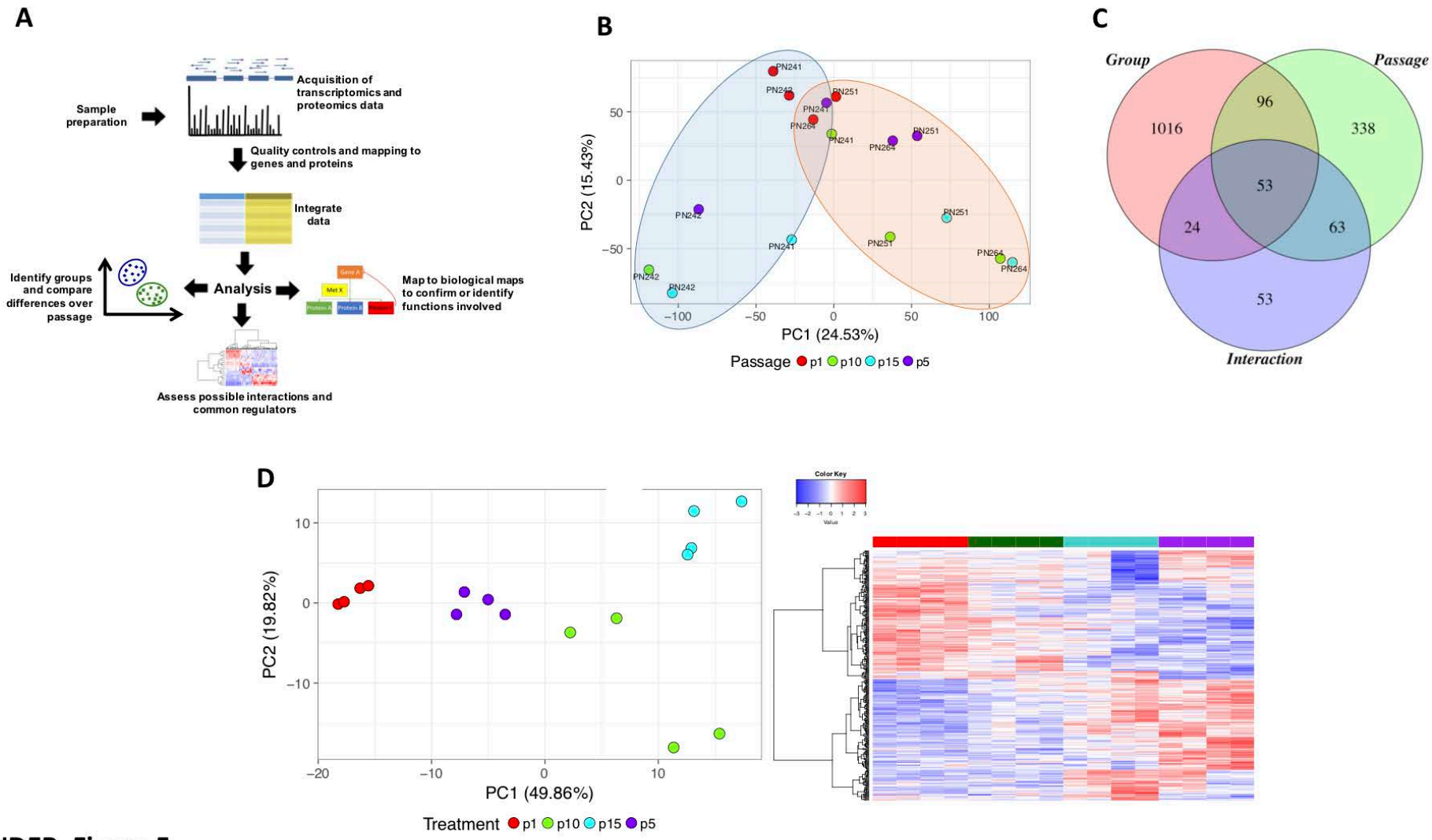

HOLLANDER Figure 5

TOP

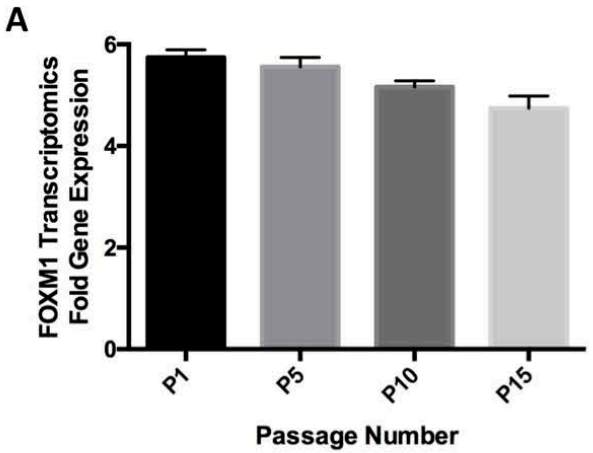

C

MOVEMENT OF MESENCHYMAL STEM CELLS		MIGRATION OF MESENCHYMAL STEM CELLS		WOUND HEALING	
Entities in term: 51 Mapped to our data: 22		Entities in term: 45 Mapped to our data:21		Entities in term: 579 Mapped to our data:295	
GENES 21	PROTEINS 8	GENES 20	PROTEINS 7	GENES 294	PROTEINS 101
Significant over passage: 0	Significant over passage: 2	Significant over passage: 0	Significant over passage: 2	Significant over passage: 13	Significant over passage: 4
Most expressed: PDGFRA, CXCL12, PDGFRB, HIF1A	Most abundant: MIF, CXCL12, PDGFRA, PDGFRB	Most expressed: PDGFRA, CXCL12, PDGFRB, HIF1A	Most abundant: MIF, CXCL12, PDGFRA, PDGFRB	Most expressed: FN1, GJA1, COL3A1, VIM, SPARC, CXCL12	Most abundant: FN1, COL1A1, SERPINE1, GSN, THBS1, COL3A1

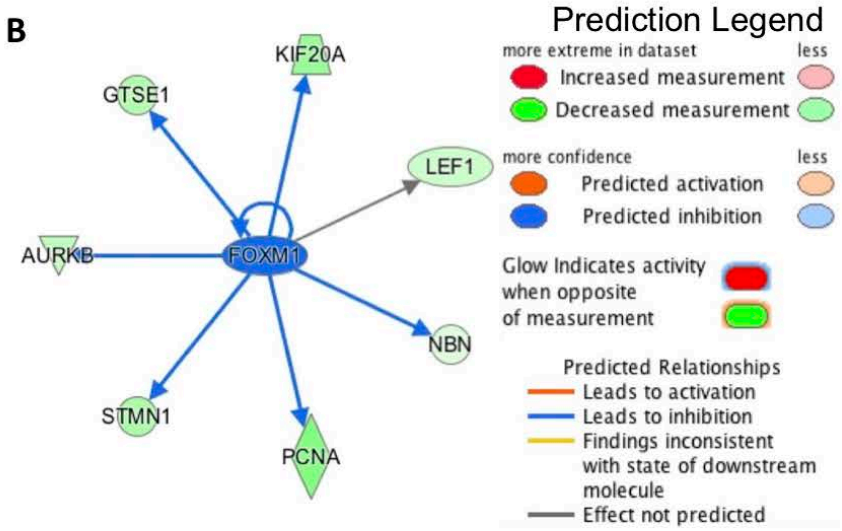

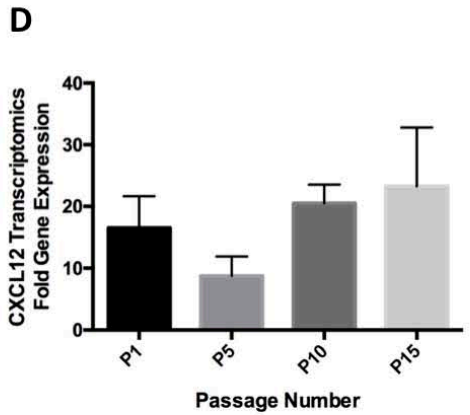

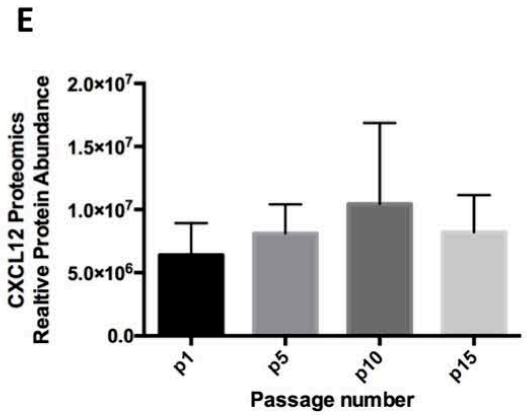

HOLLANDER Figure 6

TOP

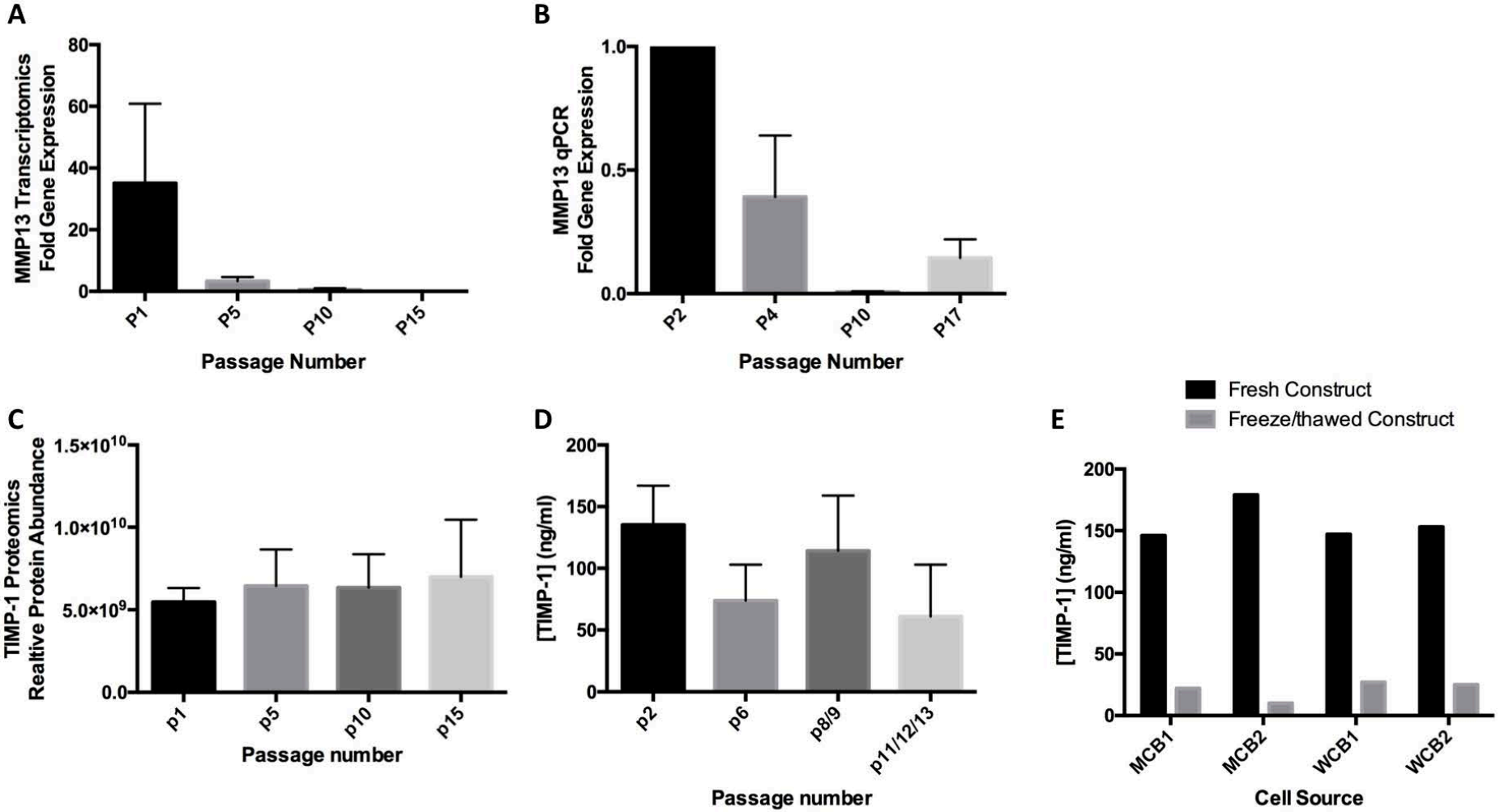

HOLLANDER Figure 7

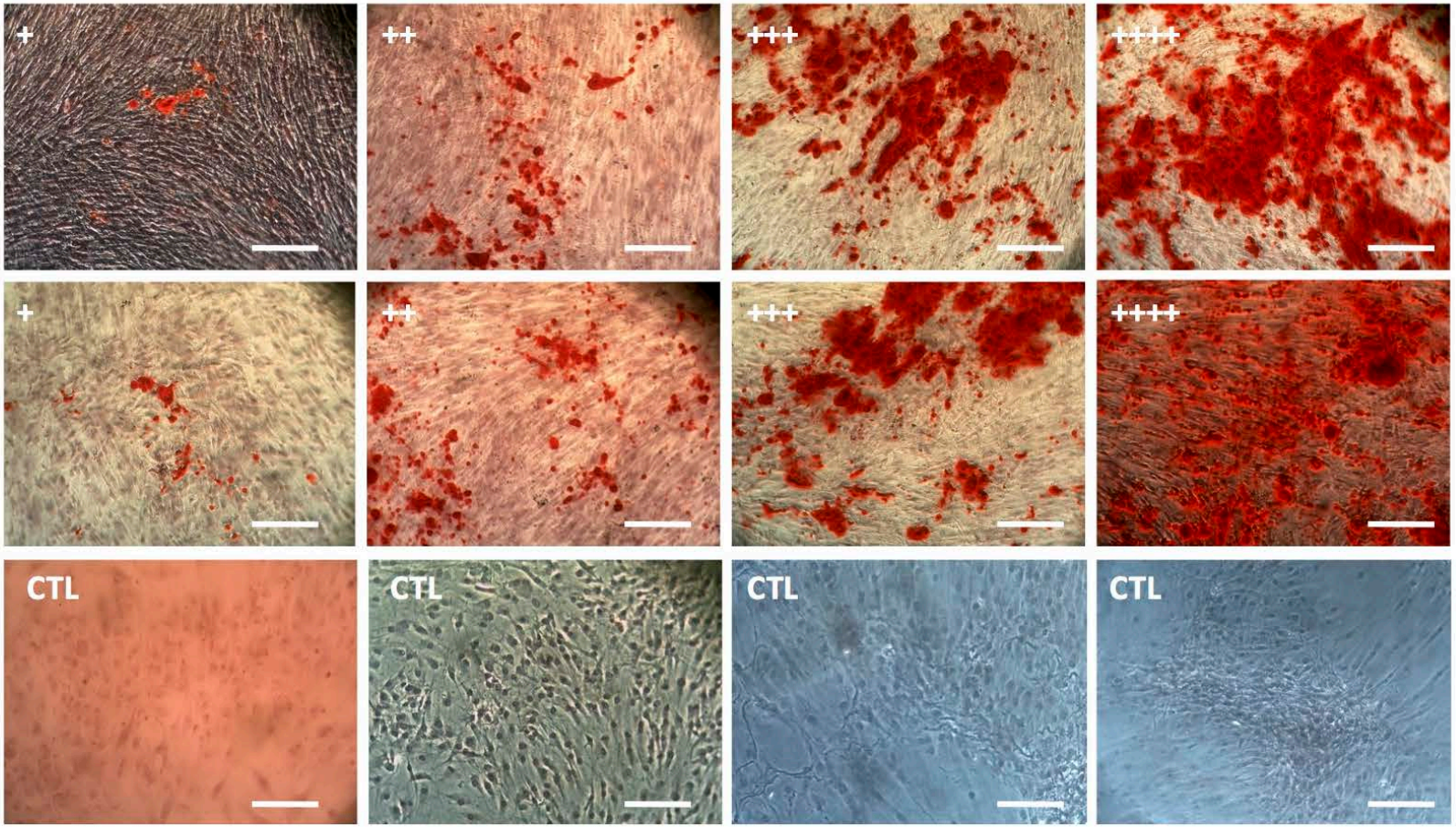

Figure S1

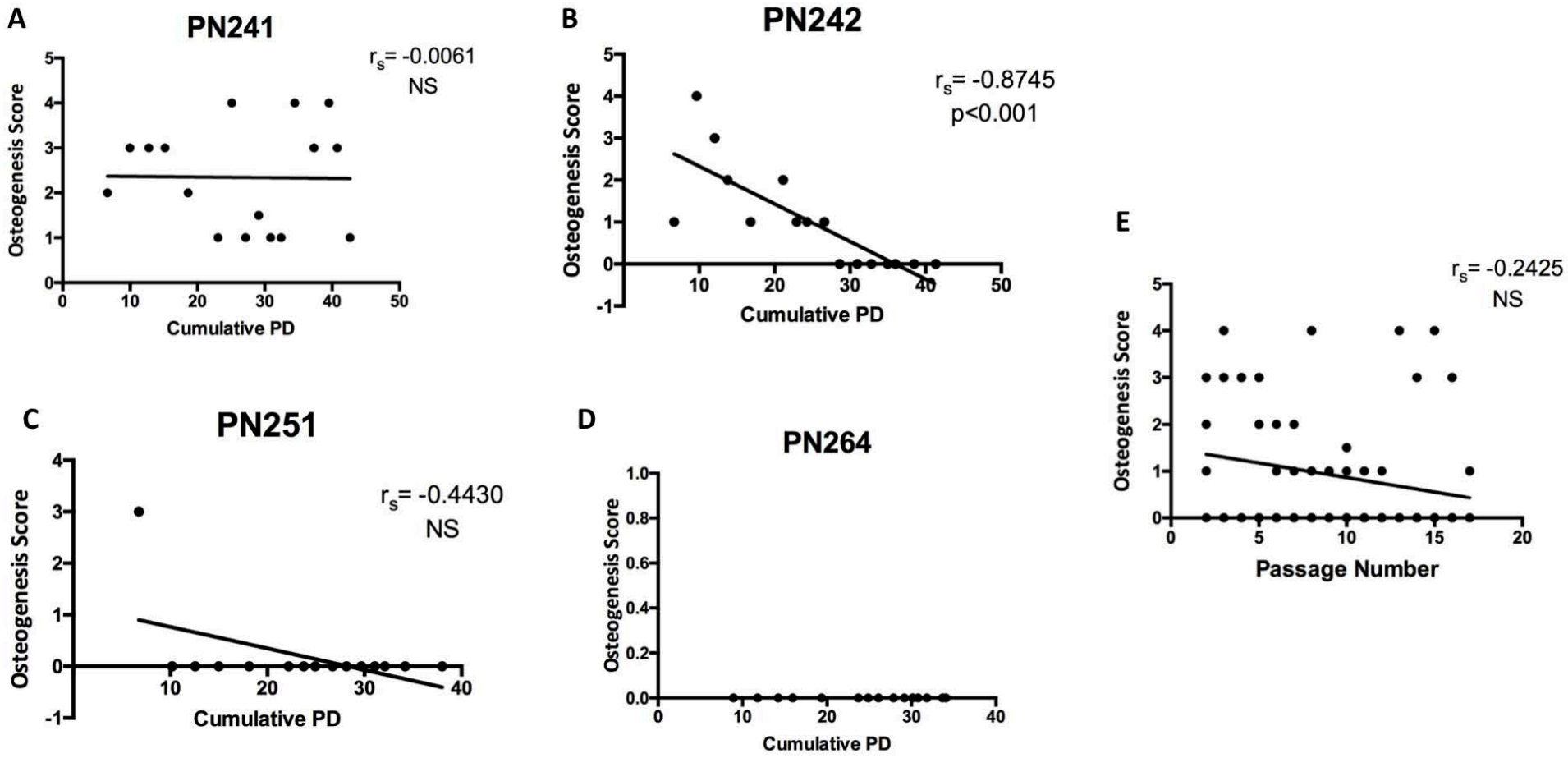
A
PN241
r_s= -0.0061
NS
Osteogenesis Score
Cumulative PD
B
PN242
r_s= -0.8745
p<0.001
Osteogenesis Score
Cumulative PD
C
PN251
r_s= -0.4430
NS
Osteogenesis Score
Cumulative PD
D
PN264
Osteogenesis Score
Cumulative PD
E
r_s= -0.2425
NS
Osteogenesis Score
Passage Number

Figure S2

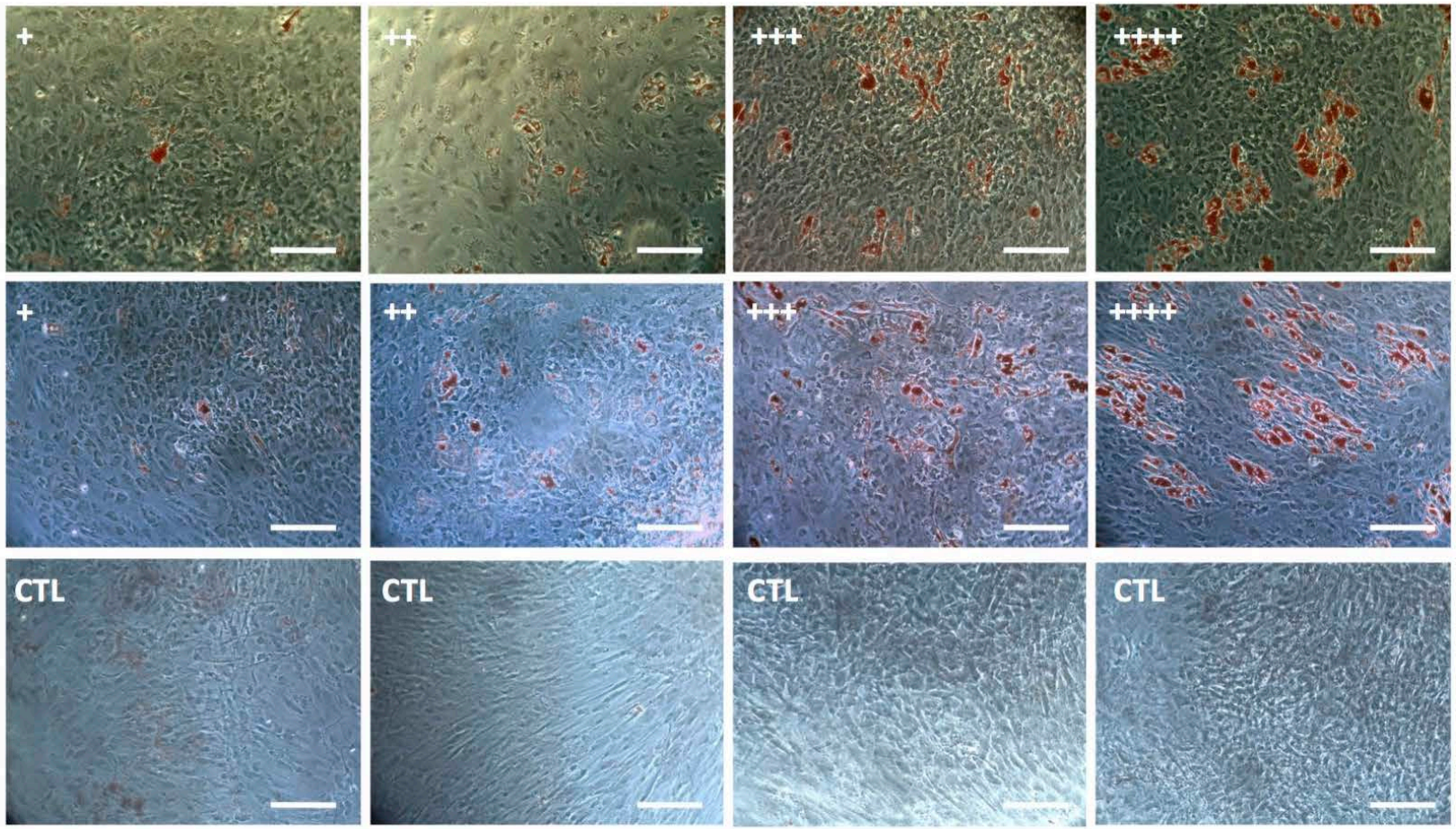

Figure S3

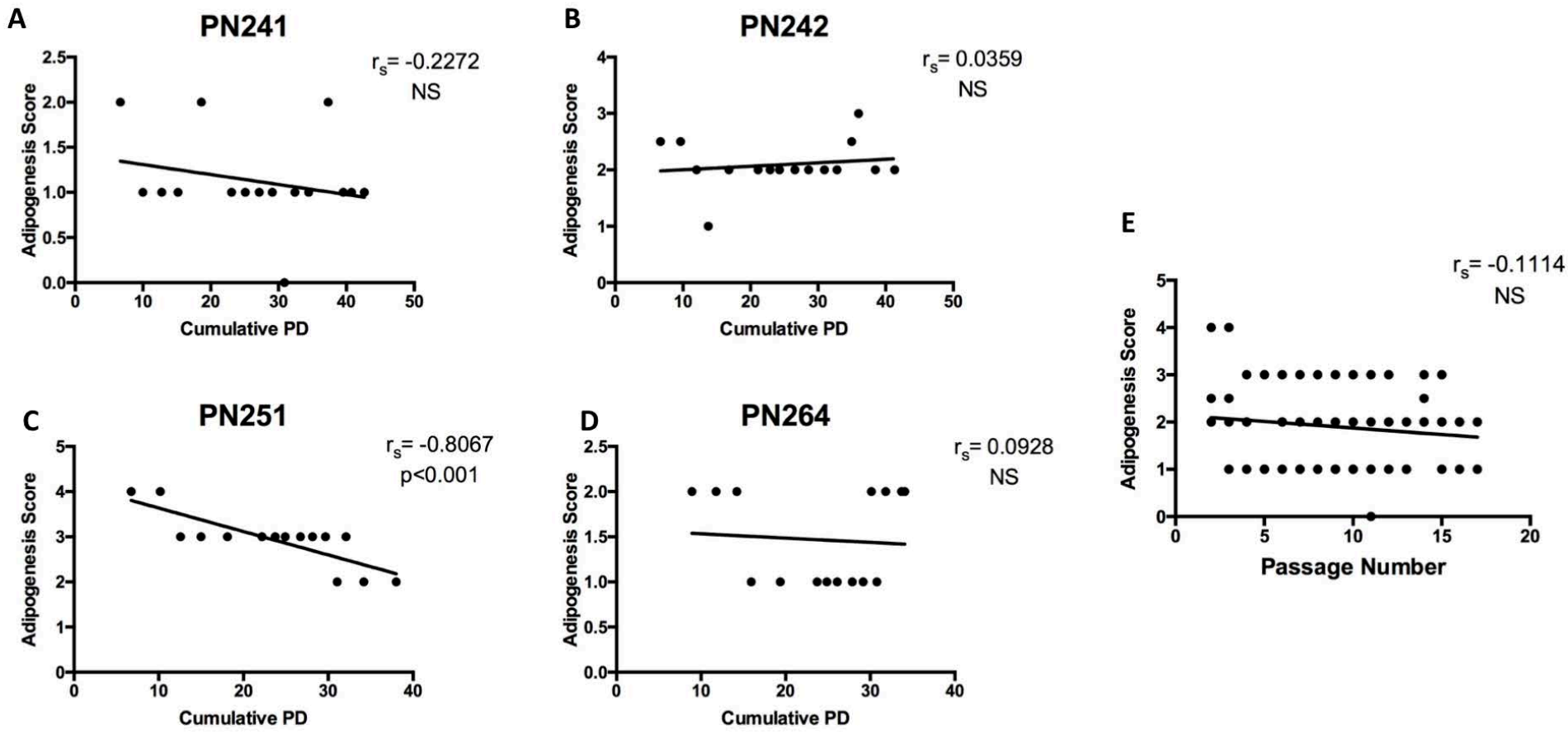
A
PN241
r_s= -0.2272
NS
Adipogenesis Score
Cumulative PD
B
PN242
r_s= 0.0359
NS
Adipogenesis Score
Cumulative PD
C
PN251
r_s= -0.8067
p<0.001
Adipogenesis Score
Cumulative PD
D
PN264
r_s= 0.0928
NS
Adipogenesis Score
Cumulative PD
E
r_s= -0.1114
NS
Adipogenesis Score
Passage Number

Figure S4

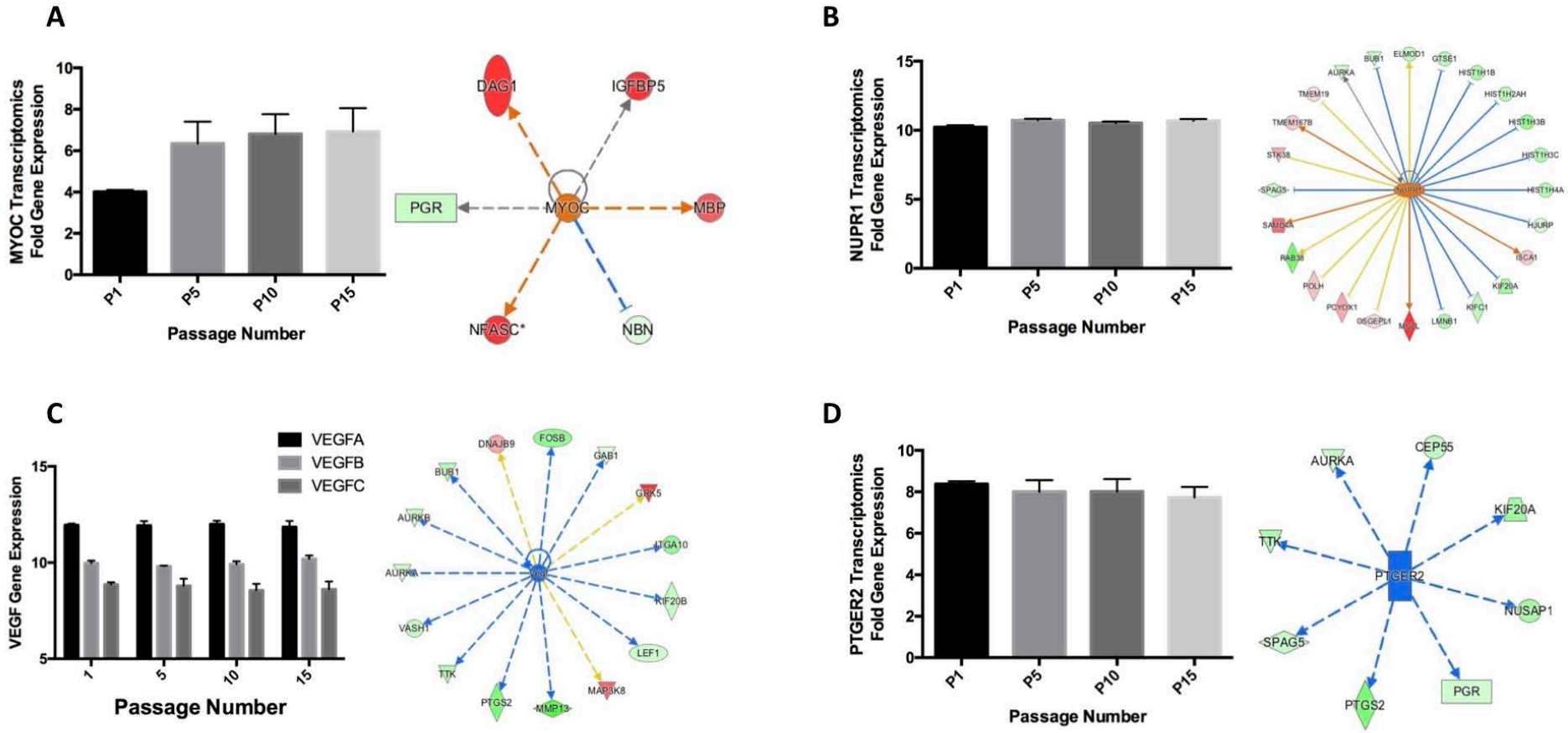
A
MYOC Transcriptomics Fold Gene Expression
Passage Number
P1
P5
P10
P15
DAG1
IGFBP5
PGR
MYOC
MBP
NFASC*
NBN
B
NUPR1 Transcriptomics Fold Gene Expression
Passage Number
C
VEGFA
VEGFB
VEGFC
VEGF Gene Expression
Passage Number
DNAJB9
FOSB
GAB1
BUB1
GRK5
AURKB
ITGA10
AURKA
KIF20B
VASH1
LEF1
TTK
MAP3K8
PTGS2
MMP13
D
PTGER2 Transcriptomics Fold Gene Expression
Passage Number
AURKA
CEP55
KIF20A
TTK
PTGER2
NUSAP1
SPAG5
PGR
PTGS2

Figure S5

Table S1. Patient details and MSC culture. Bone marrow was obtained from each of four donors undergoing surgery following traumatic injury. Growth arrest was recorded as the last Passage at which an increase in cell number was recorded. Cells from PN242 continued to proliferate at P30, after which the experiment was terminated.

Donor	Age at surgery (Years)	Gender	MSC passage at growth arrest
PN241	45	M	P25
PN242	38	M	>P30
PN251	70	M	P17
PN264	43	M	P16

Table S2. Mean gene expression levels at each passage from transcriptomic data relating to matrix metalloproteinase family genes. ANOVA was used to test significant variation from P1 through to P15. Significant changes highlighted with red text.

Gene	p1	p5	p10	p15	ANOVA P value
MMP1	5.5998732	5.79613531	4.95625731	5.65660047	0.99307064
MMP11	7.86223562	7.68306861	7.18984412	6.9289258	0.37797616
MMP13	10.0768097	7.88922323	5.6507086	5.1051077	0.0392376
MMP14	14.1920592	14.0462124	14.0181522	13.7617206	0.10282711
MMP15	6.62219651	6.6322322	6.09832576	5.87278483	0.09315796
MMP16	9.47449366	9.70117959	9.13228025	9.1221298	0.71596372
MMP17	6.61458779	6.45119928	6.42559403	6.25754062	0.9183799
MMP19	7.89561958	7.81847612	7.78299404	7.52317205	0.41654145
MMP2	13.9744784	13.985333	13.9381087	13.9339775	0.99943649
MMP24	6.21874088	6.44035293	6.60509831	6.39380761	0.58978511
MMP24-AS1	7.33276168	7.56962075	7.54026812	7.37038882	0.69985261
MMP25	1.43714412	1.40793236	1.79394523	1.56026113	0.58544464
MMP28	4.78786145	4.64276263	4.87752538	4.81640313	0.97791831
MMP3	3.54205151	2.89678063	2.90764104	3.09622363	0.32241168

Table S3. Mean gene expression levels at each passage from transcriptomic data relating to insulin-like growth factor family genes. ANOVA was used to test significant variation from P1 through to P15. Significant changes highlighted with red text.

Gene	p1	p5	p10	p15	ANOVA P value
FIGF	1.766388704	1.785539917	1.561268748	1.784696387	0.872544153
IGF1	8.36150045	7.853231912	7.9100807	6.95961508	0.682343942
IGF1R	9.525628717	9.623276784	9.835460052	9.984616432	0.273174169
IGF2	1.797574755	1.942635003	2.060736917	1.87051458	0.850417613
IGF2-AS	2.392545163	2.82090428	2.981375358	2.529064565	0.580132182
IGF2BP1	4.993120303	5.23977081	6.051077551	5.888056299	0.604856443
IGF2BP2	8.491727488	8.711832275	8.387332288	8.447843126	0.15209104
IGF2BP3	6.772587378	6.564516998	6.566581798	6.63153097	0.996849241
IGF2R	10.64727025	10.93571433	10.89836614	10.97222435	0.344377129
IGFALS	0.97232465	0.955956548	1.252926517	0.946706521	0.26398872
IGFBP1	2.818366246	2.85717034	2.700755194	3.569848744	0.427416333
IGFBP2	9.671513003	10.5682349	10.87819621	11.17326522	0.634062901
IGFBP3	14.31915607	14.59662532	14.56390172	15.19442393	0.67135429
IGFBP4	11.28057242	11.64997926	11.78187461	11.53089188	0.781250375
IGFBP5	12.79305878	13.51606844	14.45217328	15.16636268	0.037020368
IGFBP6	12.68995546	12.73214007	13.09245732	12.99015695	0.831659325
IGFBP7	11.57745438	11.14780103	11.04839444	11.01817982	0.968411897
IGFBP7-AS1	2.505413873	2.487770296	2.564428641	2.463306097	0.987864613
IGFBPL1	1.560575075	1.821169981	1.712299146	1.550038652	0.6999863
IGFLR1	4.811177986	4.574514281	4.343826906	4.561327033	0.841321237
PIGF	6.418983207	6.635966057	6.37149974	6.611985474	0.467353007

Table S4. Mean gene expression levels at each passage from transcriptomic data relating to Transforming Growth Factor β genes. ANOVA was used to test significant variation from P1 through to P15. No significant changes were observed

Gene	p1	p5	p10	p15	ANOVA P value
CTGF	12.93129068	13.11114526	12.95890603	13.78806378	0.236277103
PTGFR	14.11406285	13.7972693	13.15233422	12.80056628	0.185256607
PTGFRN	10.48101411	10.51169203	10.6445946	10.72228582	0.98685427
TGFA	2.720032823	2.436113251	1.972078689	2.588237911	0.499795593
TGFB1	6.727452624	6.543144794	6.651820715	6.426532051	0.820938007
TGFB1I1	8.20127917	8.092501175	7.928413536	7.684186941	0.292599591
TGFB2	9.038249337	9.530277765	9.524899648	10.15981589	0.366663633
TGFB3	10.16573317	9.227449618	8.585776596	8.340849151	0.123002756
TGFBI	14.23009913	14.17688001	14.05364426	13.94196898	0.928362048
TGFBR1	12.59078859	12.81077217	13.11977441	13.19717954	0.642588238
TGFBR2	12.53651792	12.61765041	12.9401318	13.29719118	0.431966177
TGFBR3	10.54188845	10.66198291	10.78132306	10.94399838	0.86251197
TGFBR3L	1.920506931	1.812601554	1.934937741	1.720610947	0.776172143
TGFBRAP1	9.487183102	9.465681952	9.654275737	9.419263045	0.572928938

Table S5. Mean protein expression levels at each passage from proteomic data for proteins abundantly expressed at all passages

Protein	p1	p5	p10	p15	Mean Expression
Metalloproteinase Inhibitor 1 (Tissue Inhibitor of Metalloproteinase 1; TIMP1)	5.47×10^9	6.45×10^9	6.35×10^9	6.99×10^9	6.31×10^9
Fibulin 1	1.95×10^9	1.50×10^9	2.30×10^9	2.26×10^9	2.00×10^9
Insulin-like growth factor binding protein 7 (IGFBP7)	9.03×10^8	1.61×10^9	1.91×10^9	2.05×10^9	1.62×10^9
Prelamin-A/C	1.46×10^9	1.47×10^9	1.50×10^9	1.48×10^9	1.48×10^9
Myosin-9	9.83×10^8	9.39×10^8	9.10×10^8	9.49×10^8	9.45×10^8
Complement C1s subcomponent	6.57×10^8	7.22×10^8	1.15×10^8	1.12×10^8	9.12×10^8
Thrombospondin-1	4.78×10^8	6.48×10^8	6.58×10^8	9.02×10^8	6.71×10^8
Filamin B	5.18×10^8	4.59×10^8	4.83×10^8	6.05×10^8	5.16×10^8
Glia-derived nexin	2.08×10^8	3.38×10^8	3.51×10^8	6.31×10^8	3.82×10^8